



Deposited via The University of York.

White Rose Research Online URL for this paper:

<https://eprints.whiterose.ac.uk/id/eprint/104956/>

Version: Accepted Version

---

**Article:**

Rofo, Adam P, Davis, Luther J, Whittingham, Jean L et al. (2016) The Rhodococcus equi virulence protein VapA disrupts endolysosome function and stimulates lysosome biogenesis. *Microbiology Open*. e00416. ISSN: 2045-8827

<https://doi.org/10.1002/mbo3.416>

---

**Reuse**

This article is distributed under the terms of the Creative Commons Attribution (CC BY) licence. This licence allows you to distribute, remix, tweak, and build upon the work, even commercially, as long as you credit the authors for the original work. More information and the full terms of the licence here:

<https://creativecommons.org/licenses/>

**Takedown**

If you consider content in White Rose Research Online to be in breach of UK law, please notify us by emailing [eprints@whiterose.ac.uk](mailto:eprints@whiterose.ac.uk) including the URL of the record and the reason for the withdrawal request.

The *Rhodococcus equi* virulence protein VapA disrupts endolysosome function and stimulates lysosome biogenesis.

Adam P. Rofe<sup>1</sup>, Luther J. Davis<sup>2</sup>, Jean L. Whittingham<sup>3</sup>, Elizabeth C. Latimer-Bowman<sup>2</sup>, Anthony J. Wilkinson<sup>3</sup> and Paul R. Pryor<sup>1,4\*</sup>

<sup>1</sup> Department of Biology, Wentworth Way, University of York, York. YO10 5DD. United Kingdom; <sup>2</sup> Cambridge Institute for Medical Research and Department of Clinical Biochemistry, University of Cambridge, Addenbrooke's Hospital, Hills Rd, Cambridge, CB2 0XY; <sup>3</sup> Structural Biology Laboratory, Department of Chemistry, University of York York. YO10 5DD, UK; <sup>4</sup> Hull York Medical School, University of York, YO10 5DD; \*Corresponding author: [paul.pryor@york.ac.uk](mailto:paul.pryor@york.ac.uk), Tel: +44 1904 328563

Short title: VapA disrupts endolysosome function

## **Summary**

*Rhodococcus equi* (*R. equi*) is an important pulmonary pathogen in foals that often leads to the death of the horse. The bacterium harbours a virulence plasmid that encodes numerous virulence associated proteins (Vaps) including VapA that is essential for intracellular survival inside macrophages. However, little is known about the precise function of VapA. Here we demonstrate that VapA causes perturbation to late endocytic organelles with swollen endolysosome organelles having reduced cathepsin-B activity and an accumulation of LBPA, LC3 and Rab7. The data are indicative of a loss of endolysosomal function, which leads cells to up-regulate lysosome biogenesis to compensate. Although there is a high degree of homology of the core region of VapA to other Vap proteins, only the highly conserved core region of VapA, and not VapD or VapG, gives the observed effects on endolysosomes. This is the first demonstration of how VapA is working and implies that VapA aids *R. equi* survival by reducing the impact of lysosomes on phagocytosed bacteria.

## Introduction

*Rhodococcus equi*, (*R. equi*) is a Gram-positive facultative intracellular pathogen with similarities to *Mycobacterium tuberculosis* (Vazquez-Boland *et al.*, 2013). Pathogenic *R. equi* infects a wide variety of animal hosts including pigs, sheep and cattle, but is most frequently associated with bronchopneumonial disease in foals and is increasingly isolated from immunocompromised humans (Topino *et al.*, 2010, Hayes *et al.*, 2011, Khan *et al.*, 2013, Nath *et al.*, 2013). Transmission of infection in foals is thought to occur through inhalation of contaminated dust or soil particles (Muscatello *et al.*, 2006). *R. equi* represents a major threat to foal health worldwide and has a significant economic impact on the horse breeding industry. Current treatments for *R. equi* infections involve combination drug therapies with rifampin and macrolides such as clarithromycin (Giguère *et al.*, 2011). These treatments can be protracted and expensive, and are not always successful. Furthermore, antibiotic resistant strains are emerging (Burton AJ *et al.*, 2013). While promising potential vaccines are in development, there are still no commercially-available vaccines (Cauchard S *et al.*, 2013) and research efforts are now focussing on the mechanisms of pathogenicity induced by *R. equi* in order to provide insights which may lead to better treatments for infection.

*R. equi* is phagocytosed by lung alveolar macrophages and becomes enclosed in an internal vacuole called the *R. equi*-containing vacuole (RCV) in which the bacterium survives. The precise character of this vacuolar compartment is unclear since there are conflicting reports on whether *R. equi* reaches the

degradative environment of the lysosome (Fernandez-Mora *et al.*, 2005, Toyooka *et al.*, 2005). It is therefore uncertain how *R. equi* is able to survive intracellularly. Eventually *R. equi* begins to multiply within the RCV, resulting in necrosis of the host cell (Luhmann *et al.*, 2004).

The ability of *R. equi* to persist and replicate intracellularly is dependent upon the presence of a ~ 90 kb virulence plasmid, which plays a crucial role in intracellular survival. Loss of the virulence plasmid renders the bacteria unable to replicate inside macrophages *in vitro* (Hondalus *et al.*, 1994, Giguere *et al.*, 1999). Avirulent strains are also cleared significantly faster in a mouse lung infection model than strains harbouring this extra chromosomal element (Gonzalez-Iglesias *et al.*, 2014). A striking feature of the virulence plasmid is the presence of a pathogenicity island containing several genes encoding virulence-associated proteins (Vaps). The expression of one of these genes in particular, VapA, has been associated with virulence *in vivo* in both mice and foals (Takai *et al.*, 1991, Giguere *et al.*, 1999). VapA has also been shown to be necessary, but not sufficient for virulence, since VapA alone can restore virulence to a Vap-A, -C, -D, -E and -F deletion mutant (Jain *et al.*, 2003) but cannot restore virulence to plasmid-cured *R. equi* strains (Giguere *et al.*, 1999). More recently, it has been shown that *vapA* along with two other genes *virR* and *virS*, are the minimum genes required to confer virulence, in the absence of the virulence plasmid (Coulson *et al.*, 2015). VirR is a LysR-type transcriptional regulator (Russell *et al.*, 2004) and VirS is an OmpR/PhoB response regulator (Kakuda *et al.*, 2014), both of which are required for proper *vapA* gene expression (Ren *et al.*, 2004). The presence of

VirR and VirS alters transcription of ~18 % of *R. equi* genes. This suggests that the plasmid is also needed to regulate chromosomal genes that may be required for intracellular growth (Coulson et al., 2015). VapA has also been demonstrated to be necessary to reduce fusion of *R. equi* containing phagosomes with lysosomes (Fernandez-Mora et al., 2005, von Bargen et al., 2009).

Sequence alignment of the different Vap proteins shows that they share a high degree of homology in the C-terminus with little homology in the N-terminus of the proteins. The crystal structures of VapB, VapD and VapG have been determined by X-ray crystallography (Geerds et al., 2014, Whittingham et al., 2014, Okoko et al., 2015) revealing that the highly conserved C-terminal region forms a tightly packed eight-stranded  $\beta$ -barrel and that the structures of these Vap proteins are superimposable. However, the crystal structures of the Vap proteins don't show any obvious ligand binding sites or grooves that would provide clues to their function. It is predicted, by homology, that VapA will have a similar structure to other Vap proteins yet there is nothing obvious in the VapA sequence that indicates why VapA is unique among the Vap proteins in being necessary for virulence.

Given the importance of VapA for *R. equi* intracellular survival we sought to determine how VapA alone affects the endocytic pathway. Our data indicate that only the  $\beta$ -barrel structure of VapA and not the  $\beta$ -barrel structure of other Vap proteins disrupts endolysosome function, promoting cells to up-regulate lysosome biogenesis to compensate for the loss of functional endolysosomes. Whilst VapA has been shown to be important for virulence, these are the first

data that demonstrate that VapA could aid *R. equi* intracellular survival by reducing cellular lysosomal function.

## **Results**

### *VapA causes swelling of late endocytic compartments*

VapA is the only Vap gene that is essential for virulence (Jain *et al.*, 2003) yet its molecular function remains unknown. Normally, phagocytosis of bacteria results in the delivery of the bacteria to lysosomes where they are destroyed by lysosomal acid hydrolases and indeed VapA has been shown to reduce fusion of the *R. equi* containing phagosome with lysosomes (Fernandez-Mora *et al.*, 2005). However, we wanted to test the hypothesis that VapA may disrupt lysosomal function *per se* thereby allowing *R. equi* to survive intracellularly. We first expressed myc-tagged VapA (under the control of a doxycycline inducible promoter) for 24 h in the cytoplasm of HeLa cells and the morphology of endocytic compartments was determined by confocal microscopy (Fig. 1). EEA1, ciMPR and LAMP1 staining (markers of early endosomes, late endosomes and lysosomes respectively) in cells expressing myc-VapA were indistinguishable from that seen in control cells. Given that *R. equi* has no known secretory system for translocating effector proteins into the host cell cytoplasm (Letek *et al.*, 2010) we also considered the possibility that VapA may aid *R. equi* survival from within the *R. equi*-containing vacuole (RCV). To test this hypothesis, VapA was produced recombinantly with either an N-terminal GST tag or a C-terminal His<sub>6</sub> tag. HeLa cells, J774.2 mouse macrophages and Normal Rat Kidney (NRK) cells were incubated with 100 µg/ml tagged-VapA, to allow VapA to be taken up by fluid-phase endocytosis. Strikingly, the late endosomes (Fig. S1) and lysosomes in these cells became enlarged and swollen (Fig. 2A,B), whereas early endocytic compartments (EEA1 positive puncta) were not affected (Fig. S1). This swollen lysosomal

phenotype was not caused by LPS endotoxin (that might be present in the VapA protein preparation) or the GST tag, as GST and LPS endotoxin had no effect on lysosome morphology (Fig. 2C). Therefore the swollen lysosomal phenotype was due to the presence of VapA. Typically, over 65% of all HeLa cells treated with VapA showed swollen lysosomes (Fig. 2D) with a 1.8-fold, a 3-fold and a 4-fold increase in lysosomal size in HeLa, J774.2 and NRK cells respectively (Fig. 2E). Thus, we aimed to characterise the effect on late endosomes and lysosomes further. *R. equi* readily infects J774.2 cells (Fig. 3A, Fig. S3) with a loss of discrete lysosomes (compared to uninfected cells), as has previously been reported (Hietala *et al.*, 1987, Zink *et al.*, 1987, von Bargen *et al.*, 2009). Although macrophages are the normal host cell for *R. equi*, the available cell line (J774.2) is not ideal for confocal analysis since all endocytic compartments are in close proximity, which hinders their analyses. Due to the spatial distribution of lysosomes in NRK cells and the greatest differences in the size of lysosomes when fed VapA we used NRK cells for subsequent studies. Whilst NRK cells do not normally phagocytose bacteria, they can be infected with *R. equi* (Fig. 3B, Fig. S3). NRK cells are infected by *R. equi* with low efficiency compared to J774.2 cells (Fig. S3). However, the bacteria are able to replicate inside NRK cells as shown by Fig. 3B, since as the Alexa-Fluor-488-labelled bacteria replicate the surface fluorescence is lost but DAPI staining of nucleic acid of replicated bacteria can be seen. At 24h NRK cells show less lysis when infected with *R. equi*, compared to mouse macrophages, with no discernable loss of lysosomes, but it is unclear as to whether this is a difference in the cell type or that NRK cells aren't as permissive for *R. equi* infection. However, infected NRK cells show swollen

lysosomes, as visualized by LGP120 (rat equivalent of human LAMP1) immunofluorescence, (Fig. 3B) mirroring the phenotype seen when VapA protein is fed to NRK, J774.2 and HeLa cells.

*The core of VapA is sufficient to cause late endosome/lysosome swelling*

Whilst the amino acid sequences of the N-terminal segment of the Vap proteins do not share a high degree of homology and are not predicted to have any tertiary structure, the remaining part of the Vap proteins (C-terminal core structure) are remarkably conserved (Fig. 4 A). Given the high degree of homology between the C-terminal core region of VapA and other Vap proteins (Whittingham *et al.*, 2014) and their identical tertiary structures (Fig. 4B), we asked whether VapD or VapG were able to induce a similar phenotype to that seen with VapA. When NRK cells were incubated with VapD-His<sub>6</sub> or VapG-His<sub>6</sub>, no swelling of lysosomal compartments was observed compared to VapA (Fig. 4C). Since the major difference between the Vap proteins is in the N-terminal segment, we hypothesised that the N-terminal region of VapA would be responsible for the observed lysosomal swelling. We therefore sought to determine whether the N-terminus of VapA was necessary to induce the swollen lysosomal phenotype, or whether the N-terminus of other Vap proteins was inhibitory to any potential function of their C-terminal core region. NRK cells were incubated with VapA lacking the N-terminal segment (VapA core) or chimeric VapA/VapD proteins (Fig. 4D). After feeding cells recombinant proteins for 24 h, the morphology of late endosomes and lysosomes was examined. Cells incubated either the VapA core protein or a VapD (N-terminal segment)-VapA core chimeric protein had enlarged late

endosomes and lysosomes. Conversely, the late endosomes and lysosomes of cells incubated with VapA (N-terminal region)-VapD core protein were identical to control cells. Thus, the N-terminal segment of VapA is not necessary for its activity and the core of VapA alone is sufficient to induce the swelling of endocytic compartments. This result was unexpected given the high degree of homology of the core region of VapA to the other Vap proteins.

*VapA induced swollen compartments accumulate intraluminal vesicles, LBPA Rab7 and LC3*

To understand further the nature of the swollen lysosomal compartment, NRK cells were pulse-chased with 10nm BSA-gold and the cells fixed for conventional electron microscopy. Electron micrographs of control cells show the BSA-gold in electron dense structures that have previously been characterized as lysosomes (Bright *et al.*, 1997) (Fig. 5A). In cells fed VapA protein, the BSA-gold was found in large electron lucent structures (up to 1 $\mu$ m across) containing numerous intraluminal vesicles (Fig. 5A). The fusion of a lysosome with a late endosome forms an endolysosome (EL) and these data suggested that VapA might be interfering with the EL, trapping material in an endolysosomal-like compartment and thus preventing lysosome re-formation. To test this hypothesis we fractionated NRK cells on a Nycodenz gradient and showed that 24h after feeding cells VapA, the lysosomal acid hydrolase  $\beta$ -hexosaminidase partially shifted to a less-dense region of the gradient (Fig. 5B). At longer time points (48h) this shift in density was not observed, which corresponds with a diminished swollen phenotype seen at this time (see later, Fig. 7). If VapA was trapping material in an EL then we might have observed the late-endosomal marker ciMPR co-migrating with the pool of less-dense  $\beta$ -

hexosaminidase-positive material at 24h. However, the converse was observed and the ciMPR was seen to migrate to a denser part of the gradient (Fig. 5C). This is consistent with immunofluorescence data where we don't see an increase in the co-localisation between late endosomes and lysosomes in the presence of VapA (Fig. 4E). However, we cannot rule out that the ciMPR can be retrieved from the swollen compartments. The idea that there is still membrane flow out of these swollen structures is confirmed by the observation that there was no cholesterol accumulation (as assessed by filipin staining) in these compartments (Fig. 5D). Further characterization of the swollen structures showed that there was an increase in the co-localisation between lysosomes (labeled with LGP110, the rat equivalent of human LAMP2) and the late-endosomal unconventional phospholipid lysobisphosphatidic acid (LBPA) (Fig. 5E, Fig. S5). The swollen compartments were also tightly associated with the late endosomal Rab protein Rab7, with very little Rab7 seen in the cytoplasm compared to control cells (Fig. 5F, Fig. S5). Consistent with earlier EEA1 data (Fig. S1), there wasn't any visible effect on the early-endosomal Rab protein Rab 5 (Fig. 5G) although the extent of colocalisation between Rab5 and LGP120 was found to increase (Fig. S5). The most dramatic effect was seen with the autophagosomal marker LC3. LC3 becomes lipidated as it associates with the luminal side of the developing autophagosomal membrane and it eventually gets delivered to the lysosome upon autolysosome formation where it gets degraded. In cells fed VapA there is an accumulation of LC3-positive puncta (Fig. 5H, Fig. S5) and these puncta are within the swollen LGP110 positive structures. Western blotting showed that VapA fed cells had a large increase

in the lipidated form of LC3 (LC3-II; Fig. 5I). To determine whether the increase in LC3-II was due to an up-regulation of autophagy or a lack of LC3-II clearance cells were also treated with Bafilomycin-A1, an inhibitor of the lysosomal V-ATPase. Bafilomycin treatment of cells did not further increase the levels of LC3-II (Fig. 5I) indicating that the increase in LC3-II was due to a lack of clearance and not an upregulation of autophagy. Together the accumulation of intraluminal vesicles, LBPA, Rab7 and LC3 in a LGP120/110 positive compartment were consistent with there being a defect in ELs.

*Endolysosomes show reduced cathepsin-B activity in the presence of VapA*

The LC3 result suggests that there is a defect in the hydrolase activity in the swollen EL compartments. Whilst we have not directly measured the pH of these swollen compartments, the swollen compartments still accumulate LysoTracker, indicating that the swollen ELs are at least acidic (LysoTracker accumulates in compartments where the pH <6.5) (Fig. 6A). Indeed, in control cells and cells fed VapD there are lysosomes that are not labeled with LysoTracker, but in cells fed VapA there are very few LGP120 positive structures that are not labeled by LysoTracker (Fig. 6A), again indicating the loss of regular lysosomes in VapA fed cells. Whether there are any subtle changes in the pH of the ELs compared to control cells is difficult to measure since in control cells there would be few ELs, we therefore assessed the hydrolase activity in cells fed VapA using the Magic Red-Cathepsin B substrate (MRCBS), which is a substrate for cathepsin B that becomes fluorescent upon cathepsin B cleavage (Pryor, 2012). In control cells and cells fed VapA or VapD there was a good MRCBS signal, with the MRCBS seen in aggregated structures in VapA fed cells (Fig. 6B). We then performed

fluorescence recovery after photobleaching (FRAP) experiments in control and VapA fed cells (Fig. 6C). In VapA fed cells there is a 35% reduction in the rate of recovery of MRCBS fluorescence after photobleaching, indicating a reduction in cathepsin-B activity (Fig. 6D). If other acid hydrolases also show this reduced hydrolytic activity then this could explain the accumulation of LBPA, Rab7 and LC3 and a swollen phenotype akin to a lysosomal storage disorder where material delivered to the lysosome is undigested.

#### *VapA induces lysosome biogenesis*

When NRK cells were incubated with VapA over a longer time course it was observed that there were more LGP120-positive puncta between 48 h and 72h (Fig. 7A). Lysosome biogenesis is known to be upregulated in response to lysosomal dysfunction (Sardiello *et al.*, 2009), which causes translocation of the transcription factor EB (TFEB) from the cytoplasm to the nucleus, resulting in a coordinated increase in expression of lysosomal genes. We hypothesised that the swollen ELs, induced by VapA, with reduced hydrolase activity would accumulate undigested material and this would result in an increase in lysosome biogenesis. NRK cells were incubated with VapA, VapD or VapG at 100 µg/ml for 8 -72 h and the resultant lysates probed by western blotting for markers of late endosomes and lysosomes (Fig. 7B). The amount LGP120, a marker of lysosomes, increased in accordance with the time cells were incubated with VapA protein. Unlike LGP120 the amount of ciMPR, a marker of late-endosomes, did not increase. Cells incubated with VapD or VapG did not show an increase in levels of LGP120.

We utilised a quantitative cytoplasm-to-nucleus translocation algorithm developed by Cellomics (Williams *et al.*, 2006) to measure the translocation of GFP- tagged TFEB into the nucleus in response to lysosomal dysfunction. NRK cells stably expressing TFEB-GFP were incubated with 100 µg/ml VapA for 8 h or 24 h. After fixing the cells, the quantitative localisation of TFEB-GFP was determined with the Cellomics ArrayScan<sup>TM</sup> widefield microscopy system and the morphology of lysosomes was analysed by confocal microscopy (Fig. 7C). After 8 h of incubation with VapA, some of the TFEB-GFP was observed to have translocated to the nucleus and swollen lysosomes could be seen. After 24 h most of the TFEB-GFP had translocated to the nucleus and the severity of the lysosomal phenotype had increased, as judged by an increase in the size of lysosomal puncta. No translocation of TFEB-GFP into the nucleus was seen in untreated control cells. In cells treated for 90 min with 250 nM Torin 1 (a potent inhibitor of the mTOR complex, which is known to cause TFEB translocation into the nucleus), the majority of the TFEB-GFP had translocated to the nucleus. TFEB-GFP expressing NRK cells were incubated with increasing amounts of VapA, VapD or VapG recombinant protein. VapA induced the translocation of TFEB-GFP to the nucleus and this was in a dose-dependent manner (Fig. 7D). However neither VapD nor VapG had any effect on TFEB. Translocation of TFEB-GFP into the nucleus was also monitored over a longer time course (Fig. 7E). In cells treated with VapA there was an increase in the amount of nuclear TFEB-GFP by 8 h with nuclear translocation being maximal at 16 to 24 h. Neither VapD nor VapG induced the translocation of TFEB into the nucleus at any time point, relative to untreated control cells. Together these results suggest that VapA causes

EL dysfunction and to compensate for the loss of lysosomes the cell up-regulates lysosome biogenesis.

## **Discussion**

The presence of the virulence plasmid in *R. equi* is widely accepted as a prerequisite for intracellular survival and replication inside eukaryotic cells (Hondalus *et al.*, 1994). The expression of VapA in particular has been associated with virulence *in vivo* in both mice and foals (Giguere *et al.*, 1999). Despite the importance of VapA in *R. equi* pathogenesis, little is known about its molecular function although it has been reported to reduce fusion of *R. equi* phagosomes with the lysosome (Fernandez-Mora *et al.*, 2005, von Bargen *et al.*, 2009) but how is unclear. A successful intracellular pathogen is often one that can avoid, or survive being delivered to, the hydrolytic environment of the lysosome. We therefore sought to determine whether VapA disrupted the lysosome itself, as a potential mechanism for allowing *R. equi* to survive intracellularly.

Some intracellular pathogens harbour type three secretion systems (T3SS), which translocate effector proteins across host-cell membranes. While *R. equi* possesses a type seven secretion system (T7SS) that allows proteins to be secreted into the RCV, there is no identified T3SS in *R. equi* to secrete proteins into the host cell's cytoplasm. In this respect, *R. equi* is similar to *Mycobacterium tuberculosis*, which also lacks a known T3SS, even though effector proteins such as SapM, PtpA and PtpB are known to act on cytoplasmic lipids and/or proteins (Saleh *et al.*, 2000, Mascarello *et al.*, 2013,

Margenat *et al.*, 2015). Given that VapA expression in the cytoplasm of HeLa cells did not cause any morphological changes to endocytic compartments, we hypothesised that the RCV represents the site of VapA activity. To test this, we cultured cells in the presence of recombinant Vap proteins, resulting in their uptake into endocytic compartments through fluid-phase endocytosis. We confirmed that recombinant protein accumulated in endocytic compartments (Fig. 2) and that VapA isn't just signaling through cell surface receptors. Importantly, we observed in a variety of cell types that when cells were fed recombinant VapA, the late endosomes/lysosomes rapidly became enlarged. Characterising this phenotype further we see large structures with intraluminal vesicles that are reminiscent of endolysosomes, with an accumulation of the late endocytic markers LBPA and Rab7 and reduced clearance of the autophagy marker LC3. These VapA-induced swollen EL compartments are still acidic, though we cannot rule out that the pH has changed, and have reduced cathepsin-B activity. The enlarged lysosome phenotype is similar to the lysosome phenotype in cells that have a lysosome storage disorder and accumulate undigested substrates. Lysosome dysfunction results in upregulation of lysosome biogenesis coordinated via the transcription factor EB (TFEB) (Sardiello *et al.*, 2009, Settembre *et al.*, 2012). We found that VapA caused lysosomal biogenesis as assessed by translocation of TFEB into the cell nucleus and western blotting for the lysosomal marker LGP120 in rat cells. The up-regulation of lysosome biogenesis is a consequence of lysosome disruption. In our system lysosomes would be lost as they become consumed in the formation of perturbed endolysosomes. This is consistent with the loss of lysosomes seen

in *R. equi* infected cells (Hietala *et al.*, 1987, Zink *et al.*, 1987). However, we then see lysosome biogenesis, which indicates a loss of lysosome function. Lysosome biogenesis is not seen in *R. equi* infected macrophages since the macrophages undergo necrosis first, in a VapA-independent manner (von Bargen *et al.*, 2009). But we do see lysosome biogenesis in J774.2 cells when fed VapA alone (data not shown).

By disrupting endolysosome function, which is essentially the phagolysosomal compartment, VapA can reduce the impact of lysosomal hydrolases and therefore can create an intracellular niche that aids *R. equi* survival. It is possible that *R. equi* phagosomes do indeed fuse with a few lysosomes, but eventually the phagolysosome becomes non-fusogenic to further lysosomal fusion, which would show up as an overall lack of delivery to many lysosomes. Our studies have only examined the role of VapA, since it is essential for virulence, but this does not preclude other factors that may aid *R. equi* virulence. For instance, similar to *M.tuberculosis*, *R.equi* has a hydrophobic cell wall containing unusual mycolic acid-containing glycolipids such as trehalose dimycolate and lipoarabinomannan (Alvarez, 2010). It has been shown that mannose-capped lipoarabinomannan disrupts traffic between the trans Golgi network and the *M.tuberculosis* phagosome, resulting in the exclusion of the vATPase (Fratti *et al.*, 2003). These lipids may play a similar role in altering the acidification of the RCV.

Our data show that VapA perturbs endolysosomes and we therefore suggest that the physiologically altered ELs are unable to digest luminal material and subsequently the compartment does not condense to re-form lysosomes. The

net result is an accumulation of undigested material and a loss of terminal lysosomes as they become consumed into the ELs. The loss of lysosomes and lysosomal function is sensed by the cell resulting in TFEB translocation to the nucleus and an increase in lysosome biogenesis (Fig. 8).

Due to the close homology in the Vaps in both sequence and structure, we considered the possibility that other Vap proteins may be able to induce the same effects as VapA. Interestingly, when NRK cells were incubated with either VapD or VapG, no changes to lysosome morphology were seen and lysosomal staining was indistinguishable from that of control cells. Although it is possible that the other Vap proteins act synergistically or are somehow modified or regulated by the activity of VapA, we found that when cells were incubated with VapD and VapG in combination, they had no effect on lysosomes (data not shown). It therefore remains unclear what the function of these additional Vaps is, considering that expression of these proteins is induced during intracellular growth (Byrne *et al.*, 2001, Ren *et al.*, 2003) and under the low pH conditions encountered in the macrophage phagosome, (Benoit *et al.*, 2001).

We also investigated which regions of VapA were responsible for its effect on lysosomes. Surprisingly, it was found that the C-terminal core of VapA alone was sufficient to induce the swollen EL structures. This was confirmed by the fact that a VapA N-terminus/ VapD core chimeric protein had no effect on lysosome morphology. Our data strongly suggest that the activity of VapA can be attributed to the core barrel structure alone. The structure of the Vap

proteins has no obvious ligand binding sites or grooves and gives no hints as to its function. As only late endocytic compartments appear to be affected it is tempting to speculate that VapA requires a decrease in pH or needs to be proteolytically processed to become active. Alternatively, VapA may interact with a host-cell component only found within the lumen of late endocytic compartments.

Together our data provide the first evidence for a likely function for VapA, namely disruption of endolysosomes, and this is likely to be a key mechanism for intracellular survival of *R. equi*. Despite the high degree of sequence homology between the Vap proteins, only VapA can disrupt the function of lysosomes. Further analysis of the differences in the C-terminal core of VapA compared to other Vap proteins should be a fruitful future route towards discovering the precise mechanism of action of this virulence protein.

## **Experimental Procedures**

*Reagents.* Mouse anti-rat LGP120 (GM10) and anti-rat LGP110 were generous gifts from Prof. Paul Luzio (University of Cambridge). Rabbit anti-VapA was a kind gift from Prof. A. Haas (University of Bonn). Mouse anti-myc antibody (9E10), rat anti-mouse LAMP1 (1D4B) and mouse anti-human LAMP1 (H4A3) were from the Developmental Studies Hybridoma Bank (DSHB, University of Iowa). ciMPR antibodies (ab124767) were from Abcam. Rabbit monoclonal antibodies to Rab5 (C8B1) and Rab7 (D95F2) were from

Cell Signaling Technology. Anti-LC3 (clone 5F10) was from Nanotools, anti-LBPA (clone 6C4) was from Merck Millipore. The plasmid for producing recombinant VapAD was a kind gift from Wim Meijer (University College Dublin). All chemical reagents and the mouse monoclonal anti- $\alpha$ -tubulin were from Sigma.

*Mammalian cell culture.* All cells were cultured in Dulbecco's modified Eagle's medium (DMEM) supplemented with 10 % (v/v) FBS, 2 mM glutamine and 1 % (v/v) penicillin-streptomycin (10 U/ml and 10  $\mu$ g/ml respectively) in a humidified 5 % CO<sub>2</sub> atmosphere at 37 °C, unless otherwise stated. Flp-In HeLa cells were a kind gift from Prof. M. Lowe (University of Manchester) and an isogenic cell line expressing myc-VapA was made by cloning myc-VapA into pCDNA5/FRT/TO and transfecting cells with this vector along with pOG44. Transfected Flp-In HeLa cells were selected with 50  $\mu$ g/ml Hygromycin B (Roche) and protein expression was induced with 1  $\mu$ g/ml doxycycline for 24h.

*Recombinant protein production.* *E. coli* (B21 DE3 pLysS) were transformed with plasmids encoding either GST- or His<sub>6</sub>-tagged proteins as appropriate. Bacteria were grown in 2 x 600 ml of LB or 2TY broth as follows: 7.5 ml of LB (plus the appropriate selective antibiotics) was inoculated with a single bacterial colony and grown overnight at 37 °C with shaking. The next day, starter cultures were diluted 1:500 into a total volume of 600 ml LB or 2TY broth, and grown at 37 °C until an OD<sub>600</sub> of 0.6 - 2.0 was obtained. Protein production was induced with IPTG to a final concentration of 0.2 mM, and cultures grown for a further 4 h. The bacteria were pelleted at 2,645 x g for 15 min at 4 °C. The cell pellet was resuspended in 10 ml of bacterial lysis buffer

(1 % (v/v) Triton X-100, 1 mg/ml lysozyme, 2 mM MgCl<sub>2</sub>, 1 U/ml DNase, in PBS) with protease inhibitors (Roche), and frozen at -20 °C overnight. The cell pellet was defrosted on ice and centrifuged at 47,800 x g in a Sorvall SS34 rotor for 20 min at 4 °C. For GST fusion proteins, the supernatant was incubated with 1 ml (packed volume) of glutathione sepharose (GE healthcare) for 1 h at 4 °C with gentle rotation. The sepharose beads were then collected and washed with 3 x 20 ml of wash buffer (1 % (v/v) Triton X-100 in PBS). GST/GST-fusion proteins were eluted with 20 ml elution buffer (50 mM Tris, pH 8.0, 10 mM reduced glutathione). These fractions were then analysed by SDS-PAGE. The eluted proteins were then pooled and dialysed extensively into PBS at 4 °C for 2 days and stored at -20 °C until needed. For the purification of His<sub>6</sub>-tagged proteins, cell pellets were processed as above. The soluble supernatant was incubated with 134 µl (packed volume) of His-Select resin (Sigma) for 1-2 h at 4 °C with gentle rotation. The beads were washed with 3 x 20 ml wash buffer (10 mM imidazole, 0.3 M NaCl, 50 mM Na<sub>2</sub>HPO<sub>4</sub>, pH8.0). Proteins were eluted with 20 ml elution buffer (250 mM imidazole, 0.3 M NaCl, 50 mM Na<sub>2</sub>HPO<sub>4</sub>, pH 8.0) and 1 ml fractions collected. Fractions were analysed by SDS-PAGE. The eluted proteins were then pooled and dialysed extensively into PBS at 4 °C for 2 days and stored at -20 °C until needed.

*Cell feeding experiments.* J774.2, NRK or HeLa cells were seeded onto glass coverslips in 24 well plates and cultured for 24 h. Cells were then incubated with the appropriate protein at 100 µg/ml for varying amounts of time. Cells were routinely rinsed three times with PBS and then fixed and processed for

confocal microscopy as described. Where cells were fed VapA in the presence of Bafilomycin-A1, the Bafilomycin-A1 concentration was 100nM.

*LysoTracker and MagicRed Cathepsin-B substrate experiments.* For LysoTracker experiments, NRK cells stably expressing LGP120-GFP (a kind gift from J. P. Luzio, University of Cambridge) were seeded onto glass bottomed 35mm dishes (MatTek Corporation) before being incubated with 100 µg/ml of recombinant VapA-His<sub>6</sub> or VapD-His<sub>6</sub> protein for 24h. The cells were then incubated with LysoTracker (as per the manufacturer's instructions) for 5 min before the LysoTracker and LGP120 were visualised on a Zeiss 880 confocal microscope. For Magic Red Cathepsin-B substrate (ABD Serotec Ltd) experiments, cells seeded onto glass bottomed dishes were incubated with or without VapA for 24 h before the medium was exchanged for medium containing the Magic Red cathepsin-B substrate (as per the manufacturer's instructions). Ten minutes after the addition of the substrate the cresyl violet fluorophore was visualized on a Zeiss 880 confocal microscope using the 561nm laser line at 2% power. For FRAP experiments, 10 images were taken before regions of interest were bleached using 50 iterations with combined laser lines 488nm at 4% power, 514nm at 2% power, 561nm at 100% power and 633nm at 0.2% power and then up to 300 images were subsequently taken with the 561nm laser line at 2% power.

*R. equi infection.* NRK and J774.2 cells were seeded onto glass coverslips and cultured for 48 h in antibiotic-free DMEM medium supplemented with 10 % (v/v) FBS (heat inactivated to 56 °C for 30 min) and 2 mM glutamine. *R. equi* was cultured overnight in BHI media with shaking at 30 °C. Bacteria were surface labeled with Alexa Fluor-488 as described ((Fernandez-Mora *et al.*,

2005). An appropriate number of bacteria were taken to infect mammalian cells at an MOI (multiplicity of infection) of 10 and resuspended in PBS. Bacteria were centrifuged onto cells at  $80 \times g$  for 5 min and incubated for 1 h at  $37^\circ\text{C}$  to allow phagocytosis of bacteria. Monolayers were rinsed 3 times with DMEM to remove unbound bacteria, and the media replaced with DMEM containing  $150 \mu\text{g/ml}$  gentamycin to kill extracellular bacteria. The cells were cultured for a further hour, and washed with PBS. The media was then replaced with DMEM containing  $10 \mu\text{g/ml}$  gentamycin, and cells cultured for 24 h to allow intracellular bacteria to grow. Cells were fixed with 4 % formaldehyde in PBS for 20 min at room temperature and then processed for immunofluorescence.

*Western blotting.* Proteins were transferred to nitrocellulose membranes using the iBlot system (Invitrogen) as per the manufacturer's instructions.

Membranes were then blocked in either 5 % (w/v) semi-skimmed milk or 5 % (w/v) BSA in TBS (100 mM NaCl, 10 mM Tris-HCl, pH 7.4) + 0.1 % (v/v) Tween-20 (TBST) for 30 min at room temperature or overnight at  $4^\circ\text{C}$ .

Membranes were probed with primary antibodies in 5 % (w/v) milk or 5 % (w/v) BSA TBST for 1 h at room temperature or  $4^\circ\text{C}$  overnight. Membranes were then washed with TBST (3 x 5 minute washes) and incubated with horseradish peroxidase conjugated secondary antibodies in milk or BSA at room temperature for 30 min. Membranes were washed a further 3 times with TBST and then proteins were visualised using ECL reagent (GE Healthcare).

*Immunofluorescence.* Cells were rinsed once with Dulbecco's PBS (Sigma) and then fixed with 4 % formaldehyde in PBS for 20 min at  $20^\circ\text{C}$  before quenching in 50 mM  $\text{NH}_4\text{Cl}$  in PBS for 10 min. For the LC3 antibody cells

were further fixed for 10 min with -20°C MeOH at -20°C. After fixation, cells were permeabilised in 0.2 % (w/v) BSA, 0.05 % (w/v) Saponin in PBS, for 10 min. All further washes and antibody dilutions were carried out in BSA/Saponin/PBS (BSP) solution. In all cases, coverslips were incubated with primary antibodies diluted in BSP for 1 h at room temperature. Coverslips were washed 3 x 5 min with approximately BSP and then incubated with Alexa fluorophore-conjugated secondary antibodies (diluted 1:300 in BSP) for 30 min, followed by a further 3 x 5 min washes with BSP. For visualisation of DNA 4',6-diamidino-2-phenylindole (DAPI) was included at 1 µg/ml in the final wash. Coverslips were rinsed once in distilled water, blotted dry, and mounted onto slides with MOVIOL 4-88 containing 2.5 % (w/v) DABCO (1,4-diazobicyclo [2,2,2]-octane). Slides were viewed on a Zeiss LSM 880 inverted confocal laser microscope running Zen software (2015) or a Zeiss LSM 510 meta Axioplan 2M upright confocal laser microscope running Zen software (2009, Carl Zeiss Ltd, Germany). Gain and laser powers were set accordingly. All images are maximum-intensity z projections unless otherwise stated. The size of puncta were determined using ImageJ and setting threshold levels to match the fluorescence, setting the scale for the image being analysed and then using the default analyze particles option.

*Electron microscopy.* 10nm BSA-gold was made as previously described (Bright *et al.*, 1997). Cells were pulsed for 4h with BSA-gold, washed with PBS and the gold chased for 4h before feeding cells VapA for 24h. Cells were then fixed with 0.1M Na cacodylate, pH 7.2, 2% (w/v) PFA and 2.5% (w/v) glutaraldehyde for 1h at 20°C. Cells were scraped and pelleted at 16,500g for 10 min. Cells were post fixed with 1% (w/v) OsO<sub>4</sub> in 0.1 M sodium cacodylate

buffer, pH 7.2, 'en bloc' stained with 0.5% (w/v) uranyl acetate in 50 mM sodium maleate buffer, pH 5.2, dehydrated in ethanol and processed for TEM in Araldite CY212 epoxy resin (Agar Scientific, Stansted, United Kingdom). Ultrathin sections (50 nm) were mounted on formvar/carbon-coated EM grids and stained with uranyl acetate and lead citrate. Sections were examined with an FEI Tecnai G2 Spirit BioTwin transmission electron microscope (Eindhoven, The Netherlands) at an operating voltage of 80 kV and images were recorded with an Eagle 4K CCD camera.

*Cellular fractionation.* NRK cells were scraped into STM buffer (250 mM sucrose, 10mM TES, pH 7.2, 1mM MgCl<sub>2</sub> and then subjected to nitrogen cavitation (Parr Instrument Company) at 500psi for 10 min. 1ml of STM buffer was used for every confluent T75 flask. The lysates were centrifuged at 1,500g for 10 min and 600µl of the post nuclear supernatant overlaid onto Nycodenz gradients consisting of 2ml 10% (w/v) Nycodenz, 2ml 16% (w/v) Nycodenz and 0.5ml 45% (w/v) Nycodenz. Nycodenz solutions were made by diluting 60% (w/v) Nycodenz with STM buffer. Gradients were centrifuged in a Beckman VTi90 rotor at 90,000rpm for 1h. Gradients were pumped off from the bottom using a long needle and a peristaltic pump, collecting approximately 27 x 190µl fractions. β-hexosaminidase was assayed as previously described (Pryor, 2016).

*TFEB experiments.* A TFEB-GFP construct in a pEGFP vector was a gift from Andrea Ballabio (Telethon Institute of Genetics and Medicine, Pozzuoli, NA, Italy) and was subcloned into a pLXIN retroviral expression vector (Clontech, Mountain View, CA, USA). A clonal NRK cell line stably expressing TFEB-GFP was generated using the pLXIN retroviral system as previously

described (Gordon et al 2009). Transduced cells of mixed expression levels were selected by culture in medium supplemented with 0.5 mg/ml Geneticin (G418) and clonal NRK cell lines expressing TFEB-GFP were subsequently generated after isolating single cells by fluorescence activated cell sorting. Nuclear translocation of TFEB-GFP was quantified after fixing with 4% (w/v) paraformaldehyde and staining nuclei with Hoechst 33342 using a Cellomics ArrayScan™ VTi high content screening, wide-field microscope with Cellomics ArrayScan™ software. After autofocussing using the Hoechst 33342 channel to detect the nuclei, the programme maps and outlines the area of each nucleus (Nuc) and a region extending outwards by an adjustable number of pixels (Cyt, representing a significant portion of the cytoplasm). Nuclear translocation is calculated as the NucCyt difference (AU, arbitrary units), which is mean fluorescence intensity in Nuc after subtracting the mean intensity of pixels in Cyt. (Mean ± SEM of 750 cells). Treatment with Torin 1 (250nM for 90min) was used as a positive control for TFEB-GFP translocation to the nucleus (Settembre et al., 2012). Images showing TFEB-GFP localization were obtained from paraformaldehyde-fixed cells using a Zeiss LSM 880 confocal microscope.

**Figure 1. VapA expression in the cytoplasm of cells has no effect on endocytic compartments.** 1  $\mu\text{g/ml}$  doxycycline was added to HeLa cells to induce expression of myc-VapA for 24 h. Cells were fixed and double labelled with myc and EEA1 (**A**), ciMPR (**B**) and LAMP1 (**C**) antibodies followed by fluorescently labelled secondary antibodies. Myc labelling is shown in red and organelle labelling is shown in green. Scale bars 20  $\mu\text{m}$ .

**Figure 2. VapA induces lysosomal swelling from within the lumen of lysosomes.** **A.** HeLa cells were incubated with or without 100  $\mu\text{g/ml}$  recombinant VapA-His<sub>6</sub> protein in the cell medium for 24 h. Cells were then fixed and double immunolabelled with  $\alpha$ -VapA antibodies and  $\alpha$ -LAMP1 antibodies followed by fluorescently labelled secondary antibodies. VapA labelling is shown in red and LAMP1 labelling is shown in green. **B.** J774.2 or NRK cells were incubated with or without 100  $\mu\text{g/ml}$  recombinant GST-VapA or recombinant VapA-His<sub>6</sub> proteins for 24h, respectively. Cells were then fixed and labelled with  $\alpha$ -LAMP1 (J774.2) or  $\alpha$ -LGP120 (NRK) antibodies followed by fluorescently labelled secondary antibodies. Scale bar 10  $\mu\text{m}$  **C.** NRK cells were incubated with 100  $\mu\text{g/ml}$  recombinant GST protein or 1  $\mu\text{g/ml}$  LPS for 24 h. Cells were then fixed and labelled with  $\alpha$ -LGP120 antibodies followed by fluorescently labelled secondary antibodies (green). Cell nuclei were stained with DAPI (blue). Scale bar 20  $\mu\text{m}$ . All images are confocal maximum intensity z-projections. Wider fields of view are shown by figure S2. **D.** Quantification of the number of HeLa cells showing swollen lysosomes Data are from a typical experiment. Numbers in parentheses represent the number of cells that were scored. **E.** Quantification of lysosomal size in HeLa, J774.2 and NRK cells in

control cells (open bars) and cells fed VapA (closed bars). Data are from a typical experiment. Numbers in parentheses represent the number of lysosomes that were counted (approximately 60 cells per condition).

**Figure 3. *R. equi* infected NRK cells show swollen lysosomal compartments.** **A.** J774.2 were seeded onto glass coverslips and cultured for 48 h in antibiotic-free DMEM medium. Cells were then infected with Alexa Fluor-488 surface-labelled *R. equi* (green) with an MOI of 10 and cells cultured for 24 h to allow intracellular bacteria to grow. Cells were fixed and immunolabelled for LAMP1 followed by a fluorescently labelled secondary antibody (red). Cell nuclei and bacterial DNA were stained with DAPI (blue). Scale bars 10  $\mu\text{m}$ . Images are confocal maximum intensity z- projections. **B.** NRK cells were infected as for J774.2 cells but lysosomes were immunolabelled with an antibody against LGP120. A region is highlighted which is magnified (bottom panels). Scale bar 10 $\mu\text{m}$ . Scale bar for the magnified image is 2 $\mu\text{m}$ . Images were acquired using a Zeiss LSM 880 with Airyscan processing and shown with a maximum intensity z-projection.

**Figure 4. The core of VapA is sufficient to cause lysosomal swelling.** **A.** Alignment of the sequences of VapA, VapD and VapG displayed together with the secondary structure elements of VapD using the programme ESPRIPT (Robert *et al.*, 2014). Invariant residues in the alignment are shown in white type on a red background; conserved residues are in blue boxes. **B.** Ribbon representation of the structures of VapD and VapG with the secondary structure elements labelled. In each case the ribbon is colour-ramped from the N-terminus (blue) to the C-terminus (red). **C.** NRK cells were incubated with

100  $\mu\text{g/ml}$  of recombinant VapA, VapD or VapG for 24 h. Cells were then fixed and immunolabelled with LGP120 antibodies followed by Alexa Fluor-488-labeled anti-mouse secondary antibodies (green). Cell nuclei were stained with DAPI (blue). Images are representative of three separate experiments. **D.** Schematic representation of recombinant chimeric Vap proteins used in cell-feeding experiments as shown by panel C. Residue numbers correspond to the full protein sequence including the signal peptide. N-term refers to the unstructured N-terminal region and C-terminal core represents the  $\beta$ -barrel 'core' structure. **E.** NRK cells were incubated with 100  $\mu\text{g/ml}$  of recombinant VapA core, VapDA or VapAD for 24 h. Cells were then fixed and double immunolabelled with LGP120 and ciMPR antibodies followed by fluorescently labelled secondary antibodies. Images are representative of two separate experiments. Scale bars 10  $\mu\text{m}$ . All images are confocal maximum intensity z-projections. Wider fields of views of immunofluorescence images are shown by figure S4.

**Figure 5. VapA feeding to cells induces the formation of large endolysosomes.** **A.** Cells were pulse-chased with 10nm BSA-gold before feeding cells with or without 100  $\mu\text{g/ml}$  VapA protein for 24h. Cells were fixed and processed for electron microscopy. Electron micrographs show the flocculated BSA-gold in control and VapA treated cells. Scale bars = 500nm. **B.** NRK cells (treated with or without VapA protein for up to 48h) were lysed using nitrogen cavitation and the lysates subjected to fractionation on a 10%-16% Nycodenz gradient. Fractions were taken from the bottom of the gradient and analysed for  $\beta$ -hexosaminidase activity. **C.** Gradient fractions (as in **B**)

were western blotted for the late endosomal marker ciMPR. **D-H.** NRK cells were incubated with or without 100 $\mu$ g/ml recombinant VapA-His<sub>6</sub> for 24h. Cells were then fixed and labelled with fillipin and LGP120 (**D**), LBPA and LGP110 (**E**), Rab5 and LGP120 (**F**), Rab7 and LGP120 (**G**) and LC3 and LGP110 (**H**). Antibodies were visualized by labeling with fluorescently labeled secondary antibodies. Scale bars 10  $\mu$ m. All images represent maximum intensity z-projections. The images in **H** were taken using a Zeiss 880 confocal microscope and had additional Airyscan processing. The right hand panels of **H** are magnifications of the indicated regions of the merge panels. **I** Western blotting of lysates for  $\alpha$ -tubulin and LC3 of cells treated with or without 100 $\mu$ g/ml VapA-His<sub>6</sub> or 100 $\mu$ g/ml VapA-His<sub>6</sub> and 100nM Bafilomycin-A1 for 24h.

**Figure 6. Cells fed VapA have reduced cathepsin-B activity.** **A.** NRK cells stably expressing LGP120-GFP (a kind gift from J. P. Luzio, University of Cambridge) were incubated with 100  $\mu$ g/ml of recombinant VapA-His<sub>6</sub> or VapD-His<sub>6</sub> protein for 24h. The cells were then incubated with LysoTracker for 5 min before the LysoTracker and LGP120 were visualised on a Zeiss 880 confocal microscope. Acidic compartments are shown by red and lysosomes by green. Scale bars are 20 $\mu$ m. Quantification of co-localisation is shown by Pearson-Spearman correlations and scatterplots as described (French *et al.*, 2008). **B.** NRK cells were incubated with or without 100  $\mu$ g/ml recombinant VapA or VapD protein for 24 h. Cells were then incubated with Cathepsin B MagicRed substrate for 10 min before imaging the site of active cathepsin B using an Andor Revolution XD spinning disk microscope. Scale bars 10  $\mu$ m.

**C.** Representative images of Magic-Red Cathepsin-B substrate in control cells and cells fed 100  $\mu\text{g/ml}$  of recombinant VapA for 24h before and after photobleaching. The photobleaching ROI is shown by boxed areas. Timings are in seconds after the start of image acquisition. **D.** Quantification of FRAP data as seen in **C**. Data are the means  $\pm$  SEM from 7-9 cells for each condition.

**Figure 7. VapA induces lysosome biogenesis.** **A.** NRK cells were incubated with 100  $\mu\text{g/ml}$  of recombinant VapA for the times indicated. Cells were then fixed and immunolabelled with LGP120 antibodies followed by fluorescently labelled secondary antibodies. Images are representative of three separate experiments. Scale bar 10  $\mu\text{m}$ . **B.** NRK cells were incubated with 100  $\mu\text{g/ml}$  of recombinant VapA-His<sub>6</sub>, VapD-His<sub>6</sub> or VapG-His<sub>6</sub> for the times indicated. Cell lysates were then western blotted for lysosomes (LGP120), late endosomes (ciMPR) and the cytoskeleton ( $\alpha$ -tubulin). 20  $\mu\text{g}$  of protein was loaded per lane. The blots are representative of three separate experiments. **C.** NRK cells expressing TFEB-GFP were incubated with 100  $\mu\text{g/ml}$  recombinant VapA for the times indicated, or with 250 nM Torin 1 for 90 min (positive control). The cells were then fixed and labelled with  $\alpha$ -LGP120 antibodies followed by fluorescently labelled secondary antibodies. Scale bar 10  $\mu\text{m}$ . **D.** NRK cells expressing TFEB-GFP were incubated with increasing concentrations of VapA, VapD or VapG for 24 h. The cells were rinsed with PBS then fixed. Cell nuclei were stained with Hoechst 33342 dye for 10 min. The cells were then scanned on a Cellomics Arrayscan plate reader to measure the translocation of TFEB-GFP from the cytoplasm to the nucleus as

described. Data is plotted as a difference of the fluorescence intensity in the nucleus compared to the cytoplasm. **E.** NRK cells expressing TFEB-GFP were incubated with 100  $\mu\text{g/ml}$  of recombinant VapA, VapD or VapG for the times indicated. The translocation of TFEB-GFP into the nucleus was measured as in D. Data are means  $\pm$  SEM (n=1, >800 cells per condition).

**Figure 8. Model of VapA action on the late endocytic pathway. A.** In normal cells late endosomes and/or autophagosomes fuse with lysosomes to form an endolysosome (EL) or an autolysosome (AL). The material delivered to the lysosome is then digested and the lysosome re-forms from the EL/AL compartment. **B.** VapA reduces the hydrolase activity in the EL/AL and material delivered to the lysosome accumulates. Lysosomes cannot be re-formed from the perturbed EL/AL causing a loss of lysosomes. The lack of functional lysosomes is sensed by the cell and TFEB signaling promotes lysosome biogenesis to compensate.

## **Acknowledgements**

We thank Paul Luzio, Nia Bryant and Katherine Bowers for critically reading the manuscript and Wim Meijer for training APR in *R. equi* culture and for the chimeric VapA/D construct. This work was supported by a studentship to APR from the BBSRC Doctoral Training Programme (BB/F016751/1) and a Department of Biology, University of York PhD enhancement award. LJD is supported by a BBSRC Industrial CASE studentship with GSK Research and Development Ltd. Support was given to JLW by a BBSRC grant (BB/J007900/1) to AJW. Further support was provided by a small project grant from the Horserace Betting Levy Board (SPrj003) to PRP. There are no conflicts of interest.

## References

- Alvarez, H.c.M. (2010) *Biology of Rhodococcus Heidelberg*, Springer.
- Benoit, S., Benachour, A., Taouji, S., Auffray, Y. and Hartke, A. (2001). Induction of vap genes encoded by the virulence plasmid of *Rhodococcus equi* during acid tolerance response. *Res Microbiol* **152**, 439-449.
- Bright, N.A., Reaves, B.J., Mullock, B.M. and Luzio, J.P. (1997). Dense core lysosomes can fuse with late endosomes and are re-formed from the resultant hybrid organelles. *J Cell Sci* **110 ( Pt 17)**, 2027-2040.
- Burton AJ, Giguère S, Sturgill TL, Berghaus LJ, Slovis NM, Whitman JL, *et al.* (2013). Macrolide- and rifampin-resistant *Rhodococcus equi* on a horse breeding farm, Kentucky, USA. *Emerg Infect Dis.* **19**, 282-285.
- Byrne, B.A., Prescott, J.F., Palmer, G.H., Takai, S., Nicholson, V.M., Alperin, D.C. and Hines, S.A. (2001). Virulence plasmid of *Rhodococcus equi* contains inducible gene family encoding secreted proteins. *Infect Immun* **69**, 650-656.
- Cauchard S, Giguère S, Venner M, Muscatello G, Cauchard J, Cohen ND, *et al.* (2013). *Rhodococcus equi* research 2008-2012: report of the Fifth International Havemeyer Workshop. *Equine Vet J.* **45**, 523-526.
- Coulson, G.B., Miranda-CasoLuengo, A.A., Miranda-CasoLuengo, R., Wang, X., Oliver, J., Willingham-Lane, J.M., *et al.* (2015). Transcriptome reprogramming by plasmid-encoded transcriptional regulators is required for host niche adaptation of a macrophage pathogen. *Infect Immun* **83**, 3137-3145.
- Fernandez-Mora, E., Polidori, M., Luhrmann, A., Schaible, U.E. and Haas, A. (2005). Maturation of *Rhodococcus equi*-containing vacuoles is arrested after completion of the early endosome stage. *Traffic* **6**, 635-653.
- Fratti, R.A., Chua, J., Vergne, I. and Deretic, V. (2003). Mycobacterium tuberculosis glycosylated phosphatidylinositol causes phagosome maturation arrest. *Proc Natl Acad Sci U S A* **100**, 5437-5442.
- French, A.P., Mills, S., Swarup, R., Bennett, M.J. and Pridmore, T.P. (2008). Colocalization of fluorescent markers in confocal microscope images of plant cells. *Nat Protoc* **3**, 619-628.
- Geerds, C., Wohlmann, J., Haas, A. and Niemann, H.H. (2014). Structure of *Rhodococcus equi* virulence-associated protein B (VapB) reveals an eight-stranded antiparallel beta-barrel consisting of two Greek-key motifs. *Acta Crystallogr F Struct Biol Commun* **70**, 866-871.
- Giguère, S., Cohen, N.D., Chaffin, M.K., Slovis, N.M., Hondalus, M.K., Hines, S.A. and Prescott, J.F. (2011). Diagnosis, treatment, control, and prevention of infections caused by *Rhodococcus equi* in foals. *J. Vet. Intern. Med.* **25**, 1209-1220.
- Giguere, S., Hondalus, M.K., Yager, J.A., Darrah, P., Mosser, D.M. and Prescott, J.F. (1999). Role of the 85-kilobase plasmid and plasmid-encoded virulence-associated protein A in intracellular survival and virulence of *Rhodococcus equi*. *Infect Immun* **67**, 3548-3557.
- Gonzalez-Iglesias, P., Scortti, M., MacArthur, I., Hapeshi, A., Rodriguez, H., Prescott, J.F. and Vazquez-Boland, J.A. (2014). Mouse lung infection model to assess *Rhodococcus equi* virulence and vaccine protection. *Vet Microbiol* **172**, 256-264.

- Hayes, D., Jr., Diaz-Guzman, E. and Hoopes, C.W. (2011). Rhodococcus equi infection after lung transplantation. *Respir Care* **56**, 1605-1607.
- Hietala, S.K. and Ardans, A.A. (1987). Interaction of Rhodococcus equi with phagocytic cells from R. equi-exposed and non-exposed foals. *Vet Microbiol* **14**, 307-320.
- Hondalus, M.K. and Mosser, D.M. (1994). Survival and replication of Rhodococcus equi in macrophages. *Infect Immun* **62**, 4167-4175.
- Jain, S., Bloom, B.R. and Hondalus, M.K. (2003). Deletion of vapA encoding Virulence Associated Protein A attenuates the intracellular actinomycete Rhodococcus equi. *Mol Microbiol* **50**, 115-128.
- Kakuda, T., Hirota, T., Takeuchi, T., Hagiuda, H., Miyazaki, S. and Takai, S. (2014). VirS, an OmpR/PhoB subfamily response regulator, is required for activation of vapA gene expression in Rhodococcus equi. *BMC Microbiol* **14**, 243.
- Khan, M.Y., Ali, S. and Baqi, S. (2013). Rhodococcus equi pneumonia in a live related renal transplant recipient. *J Pak Med Assoc* **63**, 635-638.
- Letek, M., Gonzalez, P., Macarthur, I., Rodriguez, H., Freeman, T.C., Valero-Rello, A., et al. (2010). The genome of a pathogenic rhodococcus: cooptive virulence underpinned by key gene acquisitions. *PLoS Genet* **6**, e1001145.
- Luhrmann, A., Mauder, N., Sydor, T., Fernandez-Mora, E., Schulze-Luehrmann, J., Takai, S. and Haas, A. (2004). Necrotic death of Rhodococcus equi-infected macrophages is regulated by virulence-associated plasmids. *Infect Immun* **72**, 853-862.
- Margenat, M., Labandera, A.M., Gil, M., Carrion, F., Purificacao, M., Razzera, G., et al. (2015). New potential eukaryotic substrates of the mycobacterial protein tyrosine phosphatase PtpA: hints of a bacterial modulation of macrophage bioenergetics state. *Sci Rep* **5**, 8819.
- Mascarello, A., Mori, M., Chiaradia-Delatorre, L.D., Menegatti, A.C., Delle Monache, F., Ferrari, F., et al. (2013). Discovery of Mycobacterium tuberculosis protein tyrosine phosphatase B (PtpB) inhibitors from natural products. *PLoS One* **8**, e77081.
- Muscatello, G., Anderson, G.A., Gilkerson, J.R. and Browning, G.F. (2006). Associations between the ecology of virulent Rhodococcus equi and the epidemiology of R. equi pneumonia on Australian thoroughbred farms. *Appl Environ Microbiol* **72**, 6152-6160.
- Nath, S.R., Mathew, A.P., Mohan, A. and Anila, K.R. (2013). Rhodococcus equi granulomatous mastitis in an immunocompetent patient. *J Med Microbiol* **62**, 1253-1255.
- Okoko, T., Blagova, E.V., Whittingham, J.L., Dover, L.G. and Wilkinson, A.J. (2015). Structural characterisation of the virulence-associated protein VapG from the horse pathogen Rhodococcus equi. *Vet Microbiol* **179**, 42-52.
- Pryor, P.R. (2012). Analyzing lysosomes in live cells. *Methods Enzymol* **505**, 145-157.
- Pryor, P.R. (2016). Isolating Lysosomes from Rat Liver. *Cold Spring Harb Protoc* **2016**, pdb prot084814.
- Ren, J. and Prescott, J.F. (2003). Analysis of virulence plasmid gene expression of intra-macrophage and in vitro grown Rhodococcus equi ATCC 33701. *Vet Microbiol* **94**, 167-182.

- Ren, J. and Prescott, J.F. (2004). The effect of mutation on *Rhodococcus equi* virulence plasmid gene expression and mouse virulence. *Vet Microbiol* **103**, 219-230.
- Robert, X. and Gouet, P. (2014). Deciphering key features in protein structures with the new ENDscript server. *Nucleic Acids Res* **42**, W320-324.
- Russell, D.A., Byrne, G.A., O'Connell, E.P., Boland, C.A. and Meijer, W.G. (2004). The LysR-type transcriptional regulator VirR is required for expression of the virulence gene vapA of *Rhodococcus equi* ATCC 33701. *J Bacteriol* **186**, 5576-5584.
- Saleh, M.T. and Belisle, J.T. (2000). Secretion of an acid phosphatase (SapM) by *Mycobacterium tuberculosis* that is similar to eukaryotic acid phosphatases. *J Bacteriol* **182**, 6850-6853.
- Sardiello, M., Palmieri, M., di Ronza, A., Medina, D.L., Valenza, M., Gennarino, V.A., *et al.* (2009). A gene network regulating lysosomal biogenesis and function. *Science* **325**, 473-477.
- Settembre, C., Zoncu, R., Medina, D.L., Vetrini, F., Erdin, S., Erdin, S., *et al.* (2012). A lysosome-to-nucleus signalling mechanism senses and regulates the lysosome via mTOR and TFEB. *EMBO J* **31**, 1095-1108.
- Takai, S., Sekizaki, T., Ozawa, T., Sugawara, T., Watanabe, Y. and Tsubaki, S. (1991). Association between a large plasmid and 15- to 17-kilodalton antigens in virulent *Rhodococcus equi*. *Infect Immun* **59**, 4056-4060.
- Topino, S., Galati, V., Grilli, E. and Petrosillo, N. (2010). *Rhodococcus equi* infection in HIV-infected individuals: case reports and review of the literature. *AIDS Patient Care STDS* **24**, 211-222.
- Toyooka, K., Takai, S. and Kirikae, T. (2005). *Rhodococcus equi* can survive a phagolysosomal environment in macrophages by suppressing acidification of the phagolysosome. *J Med Microbiol* **54**, 1007-1015.
- Vazquez-Boland, J.A., Giguere, S., Hapeshi, A., MacArthur, I., Anastasi, E. and Valero-Rello, A. (2013). *Rhodococcus equi*: the many facets of a pathogenic actinomycete. *Vet Microbiol* **167**, 9-33.
- von Bargen, K., Polidori, M., Becken, U., Huth, G., Prescott, J.F. and Haas, A. (2009). *Rhodococcus equi* virulence-associated protein A is required for diversion of phagosome biogenesis but not for cytotoxicity. *Infect Immun* **77**, 5676-5681.
- Whittingham, J.L., Blagova, E.V., Finn, C.E., Luo, H., Miranda-CasoLuengo, R., Turkenburg, J.P., *et al.* (2014). Structure of the virulence-associated protein VapD from the intracellular pathogen *Rhodococcus equi*. *Acta Crystallogr D Biol Crystallogr* **70**, 2139-2151.
- Williams, R.G., Kandasamy, R., Nickischer, D., Trask, O.J., Jr., Laethem, C., Johnston, P.A. and Johnston, P.A. (2006). Generation and characterization of a stable MK2-EGFP cell line and subsequent development of a high-content imaging assay on the Cellomics ArrayScan platform to screen for p38 mitogen-activated protein kinase inhibitors. *Methods Enzymol* **414**, 364-389.
- Zink, M.C., Yager, J.A., Prescott, J.F. and Fernando, M.A. (1987). Electron microscopic investigation of intracellular events after ingestion of *Rhodococcus equi* by foal alveolar macrophages. *Vet Microbiol* **14**, 295-305.

## Supplemental figure legends

**Figure S1. Feeding HeLa cells recombinant VapA causes swelling of late endosomes but not early endosomes. A.** HeLa cells were incubated with or without 100 µg/ml VapA-His<sub>6</sub> for 24 h. Cells were then fixed and labelled with anti-ciMPR and anti-VapA antibodies followed by fluorescently labelled secondary antibodies. Scale bar 20 µm. All images are confocal maximum intensity z-projections. **B.** NRK cells were incubated with or without 100 µg/ml VapA-His<sub>6</sub> for 24 h. Cells were then fixed and labelled with EEA1 and LGP120 antibodies followed by fluorescently labelled secondary antibodies. Scale bar 20 µm. All images are confocal maximum intensity z-projections.

**Figure S2. VapA induces lysosomal swelling in a variety of cell types. A.** Immunofluorescence staining of lysosomes in cells (HeLa, J774.2 and NRK) treated with or without VapA (as figure 2). Images are single confocal slices. Scale bars 10µm. **B.** Immunofluorescence staining of lysosomes in NRK cells fed GST or LPS (as figure 2). Single confocal slice. Scale bars 10µm.

**Figure S3. J774.2 and NRK cell infection with *R. equi*. A.** Control J774.2 cells (top panels) immunoabelled for LAMP1 (red) and nucleic acid stained with DAPI (blue). Bottom panels show cells infected with Alexa Fluor-488-labelled *R. equi*. Scale bars 10µm. **B** As J774.2 cells in **A** but using NRK cells and labeling lysosomes with an antibody raised against LGP120 (red). Bacteria are shown by closed arrowheads. Scale bars 10µm. **C** Typical infection rates of NRK and J774.2 cells with *R. equi* at a MOI of 10. Numbers in parentheses represent the number of cells analysed. n=1

**Figure S4. Determining the regions of VapA required for lysosomal swelling.** **A.** Immunofluorescence of NRK lysosomes in cells treated with VapA, VapD and VapG (as figure 4C). Scale bars 10 $\mu$ m. **B.** NRK cells were incubated with 100  $\mu$ g/ml of recombinant VapA core, VapDA or VapAD for 24 h. Immunofluorescence shows the LGP120 (as figure 4E). Scale bars 10 $\mu$ m.

**Figure S5. Localisation of endocytic markers in cells treated with VapA.** Immunofluorescence in NRK cells of LBPA, Rab 5, Rab7 and LC3 and lysosomes (LGP120 or LGP110) in cells treated with or without VapA. Colour of the text indicates the colour of the protein. Quantification of the degree of colocalisation of the two fluorophores of the images shown.  $\rho$ = Pearson's correlation coefficient,  $s$ = Spearman's correlation coefficient (French *et al.*, 2008). Scale bars 10 $\mu$ m.

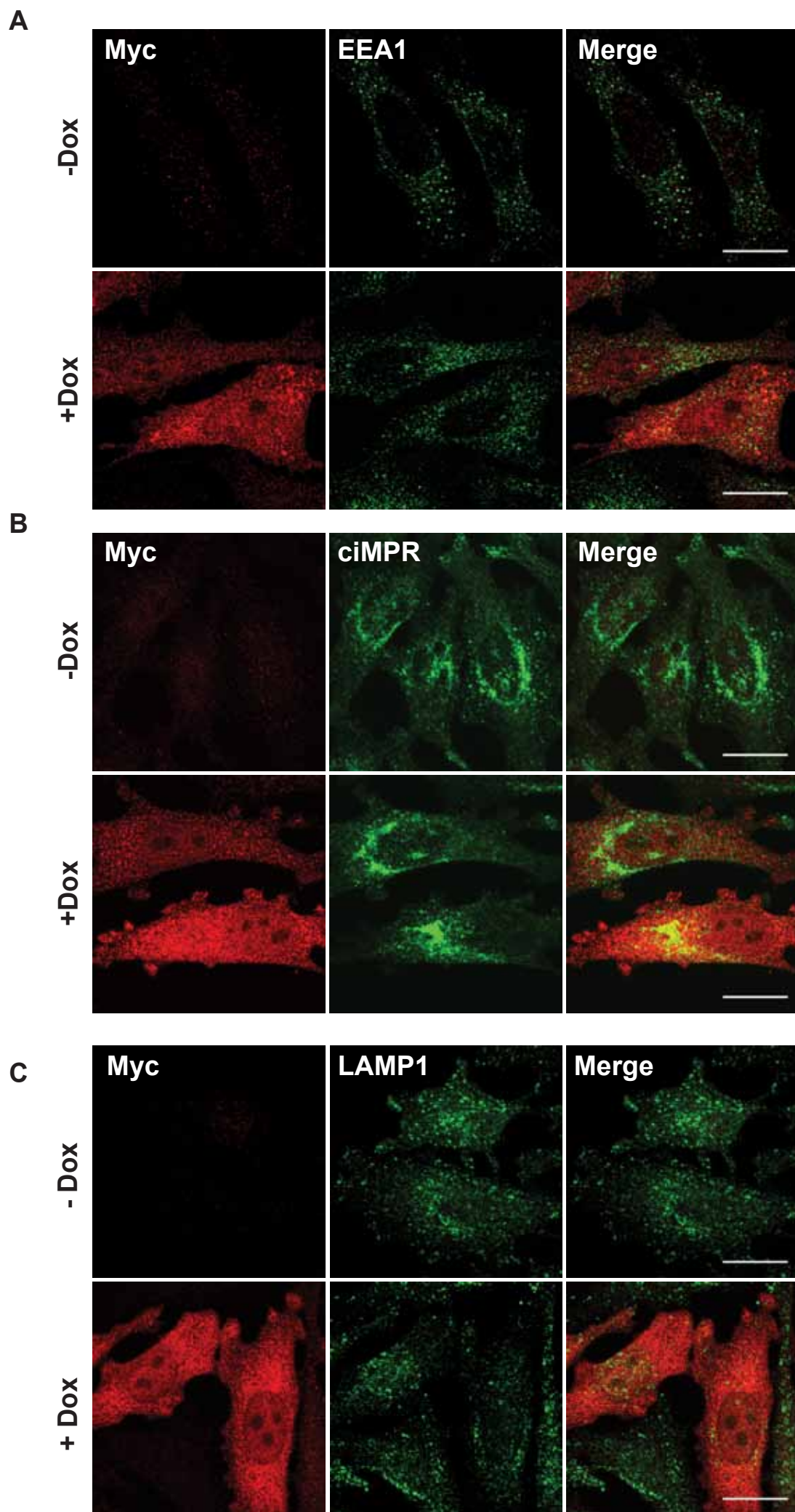
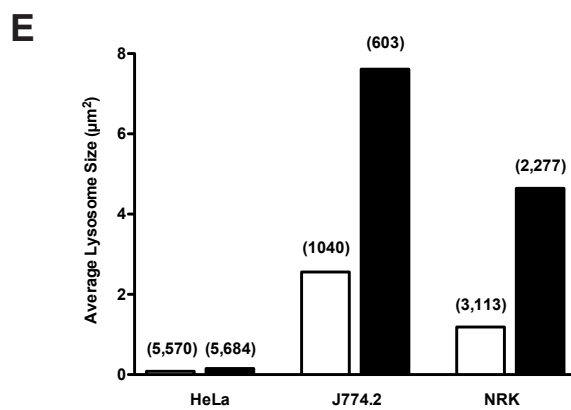
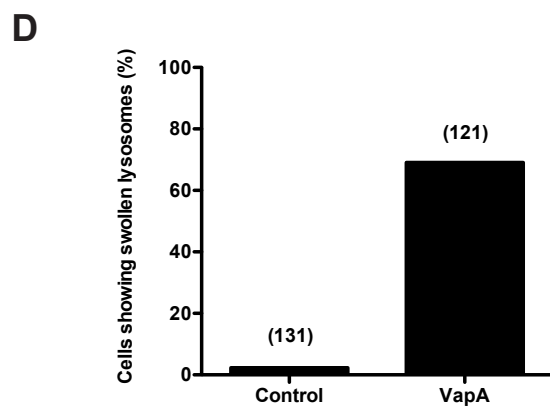
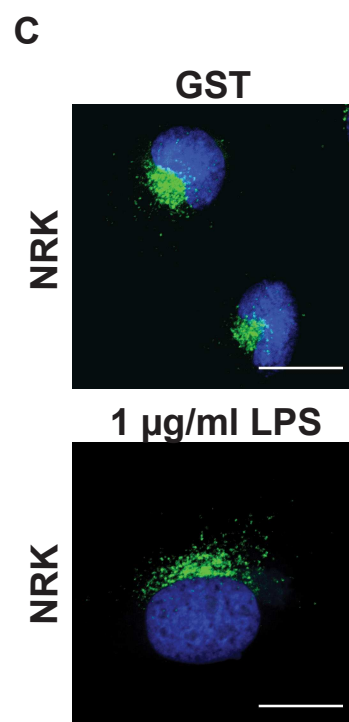
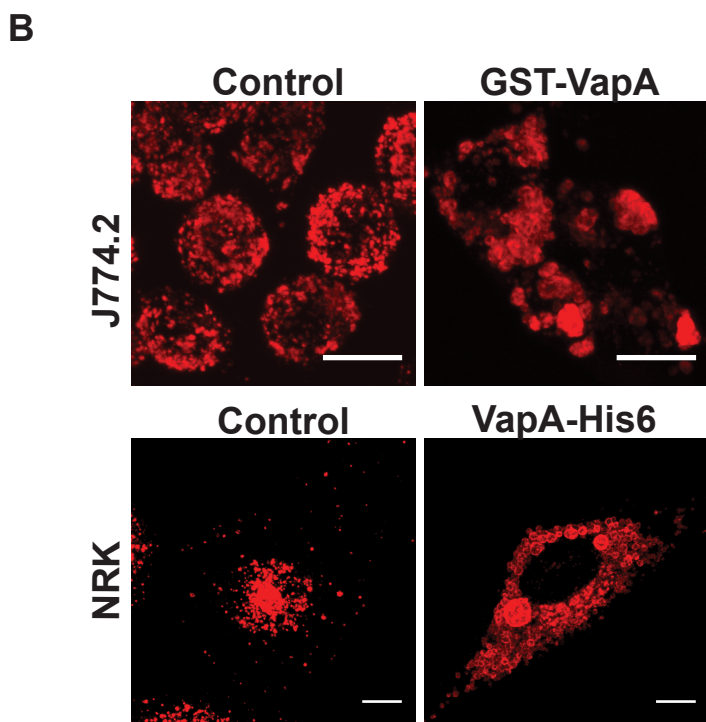
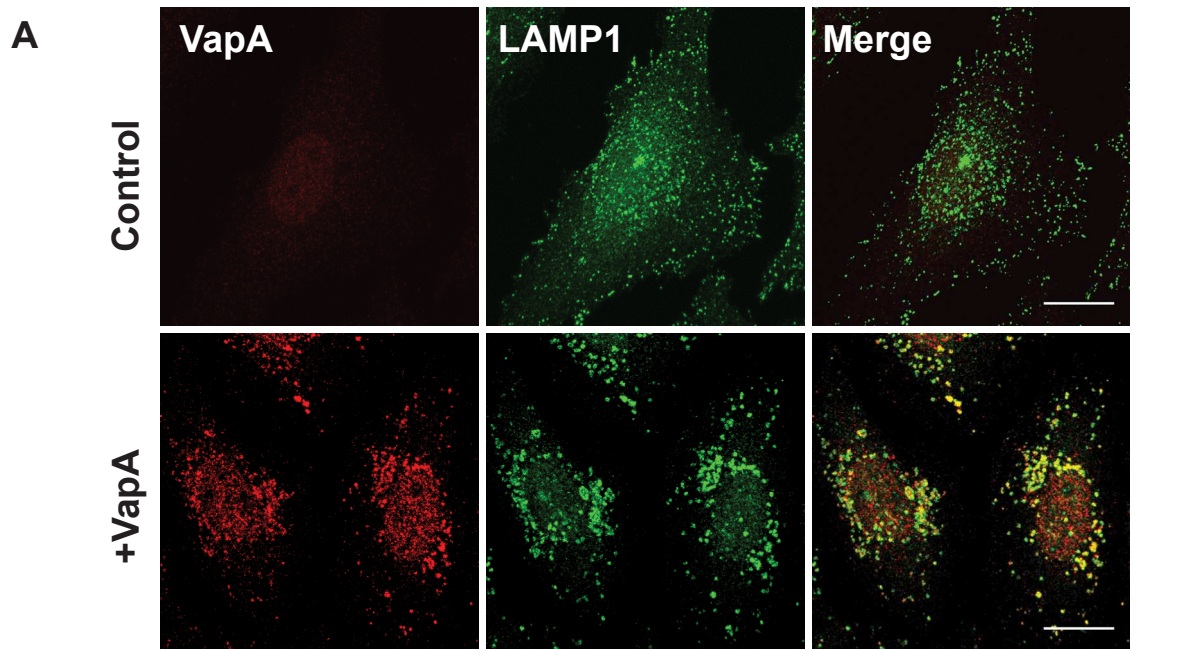
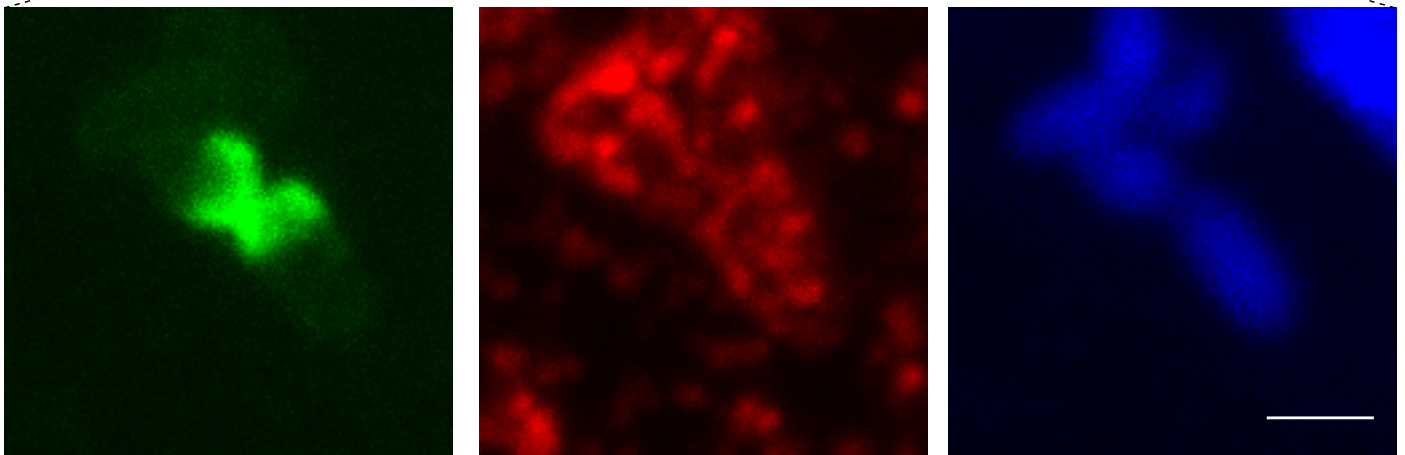
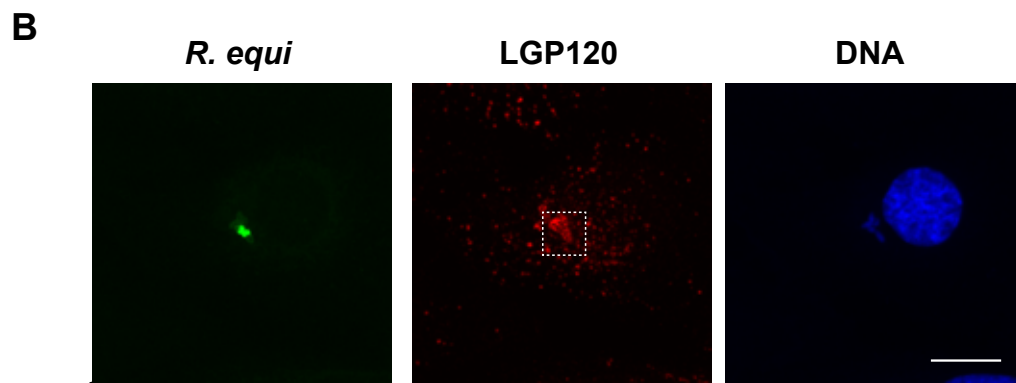
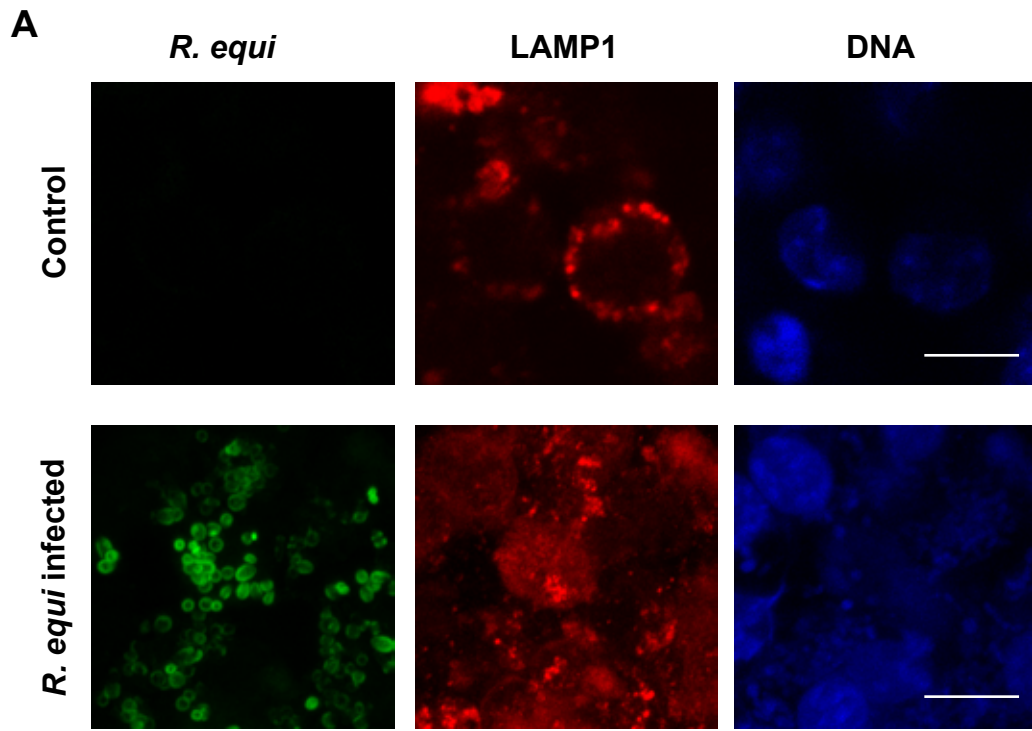


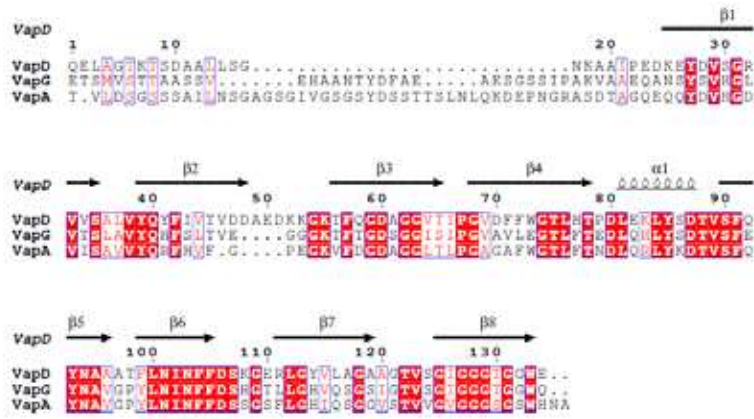
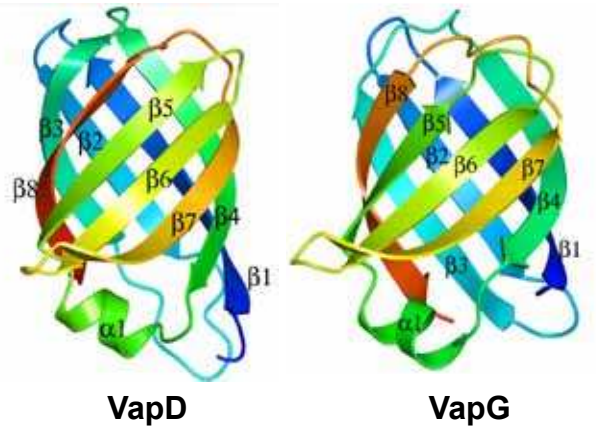
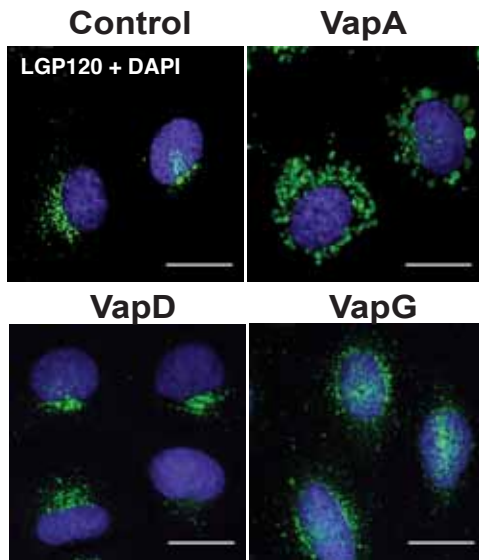
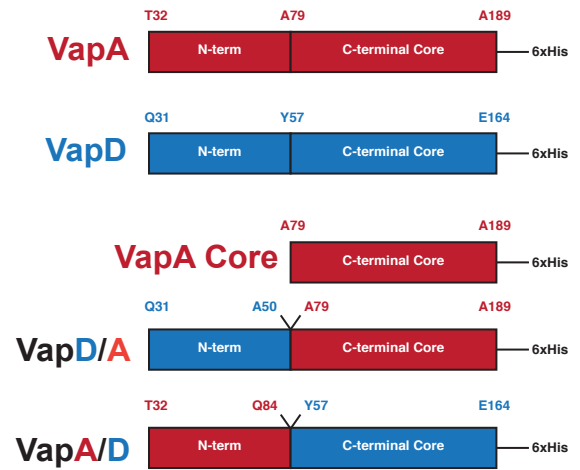
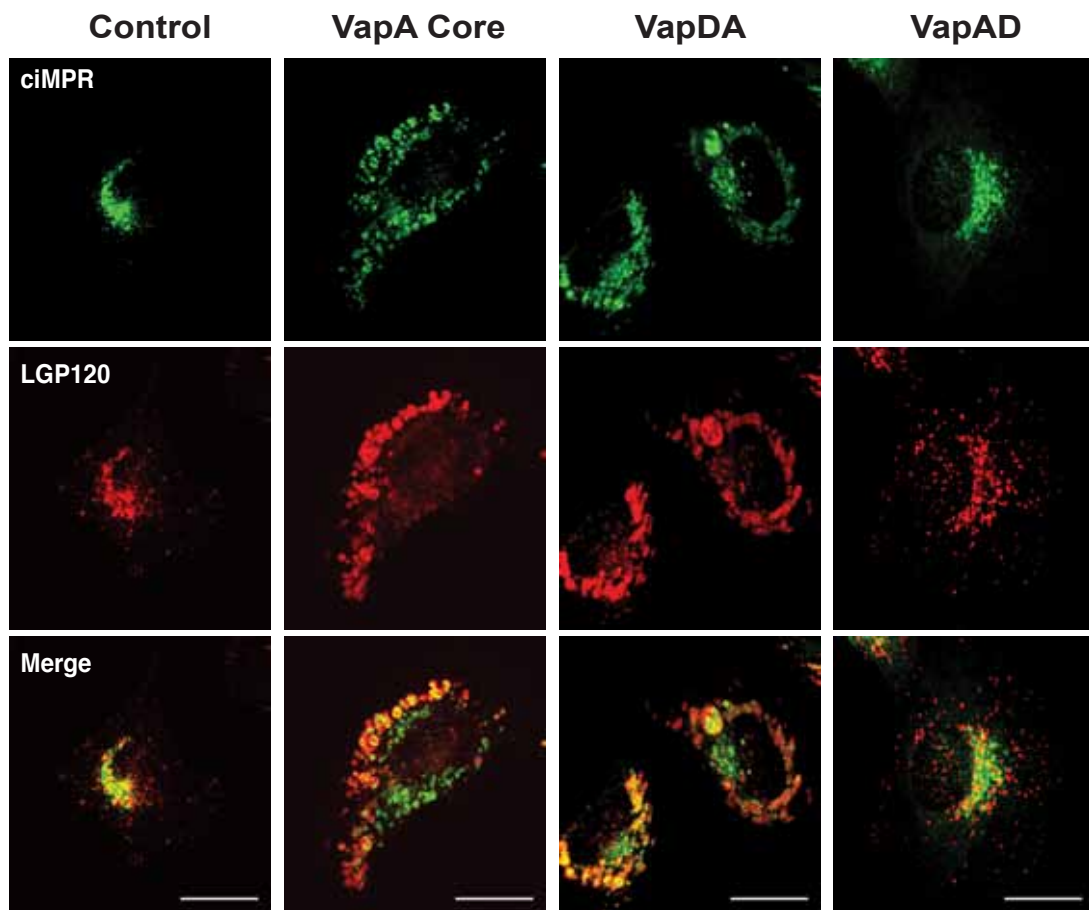
Fig. 1



**Fig. 2**



**Fig. 3**

**A****B****C****D****E****Fig. 4**

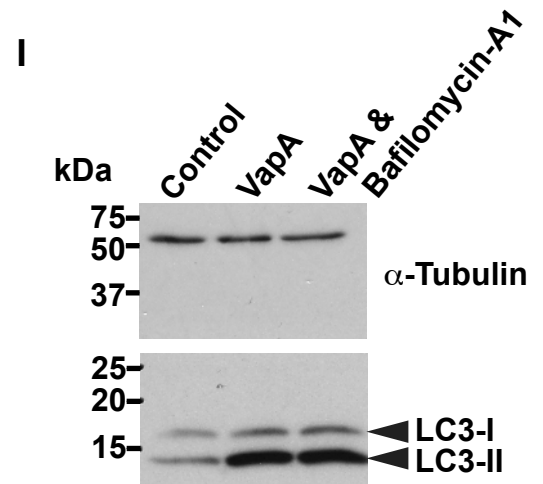
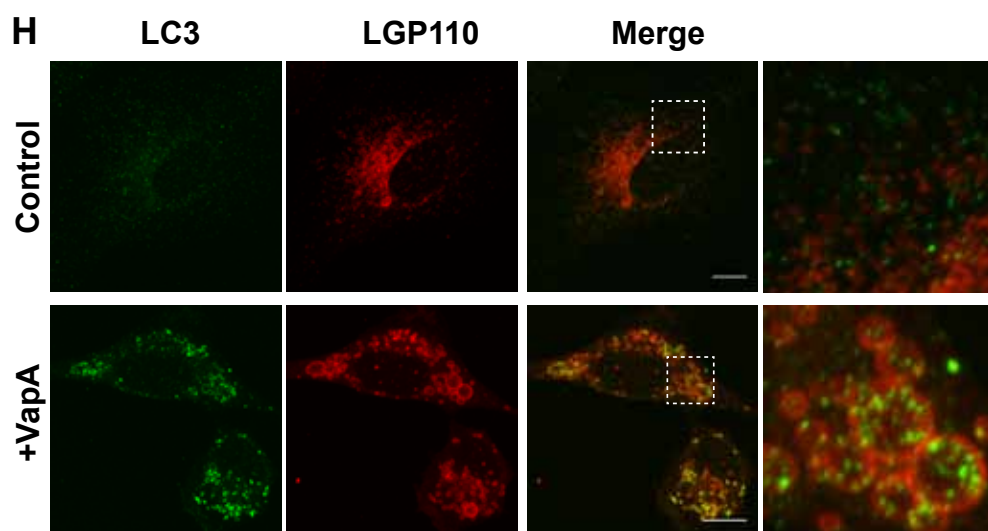
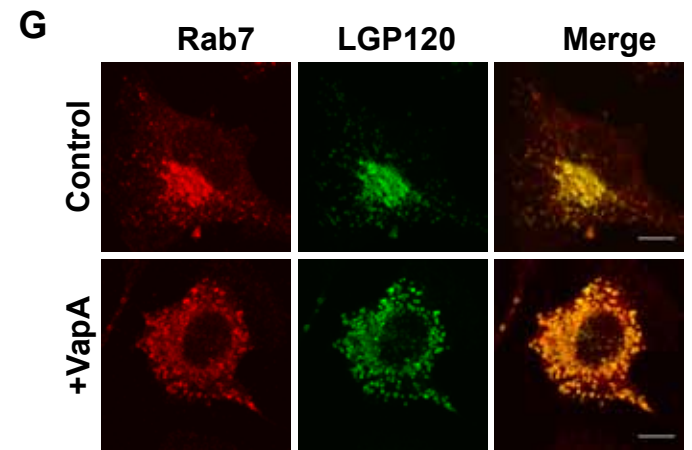
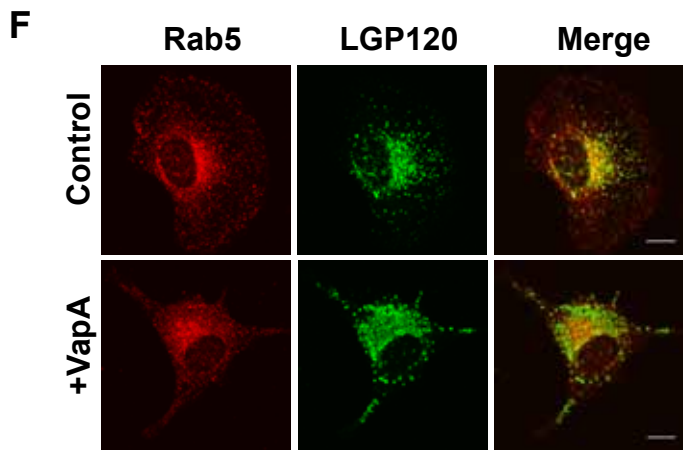
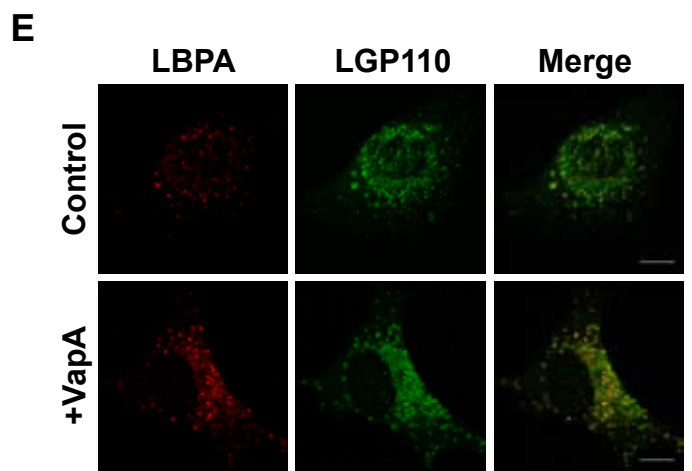
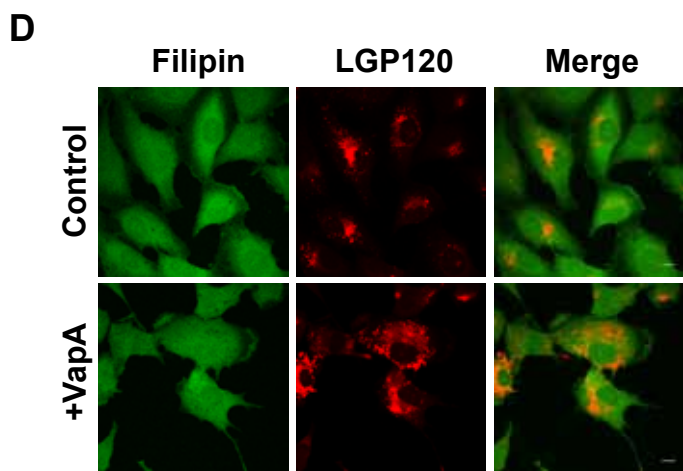
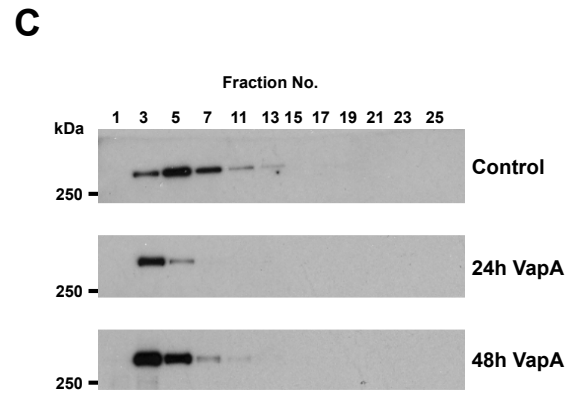
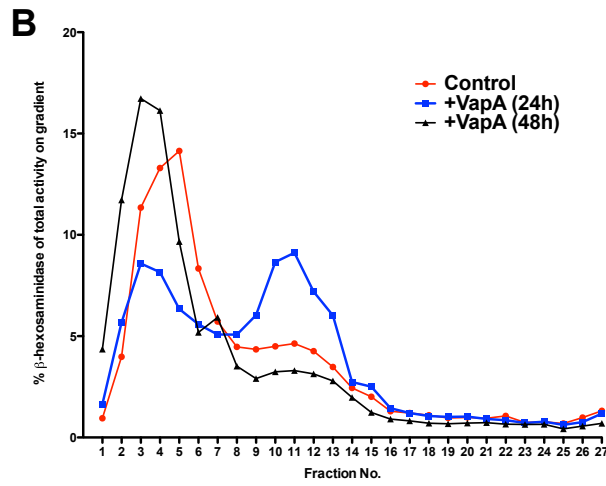
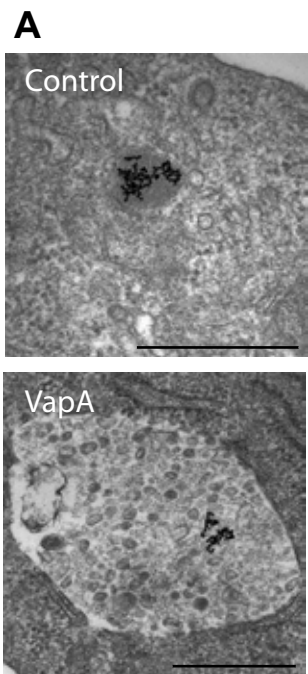


**Fig. 5**

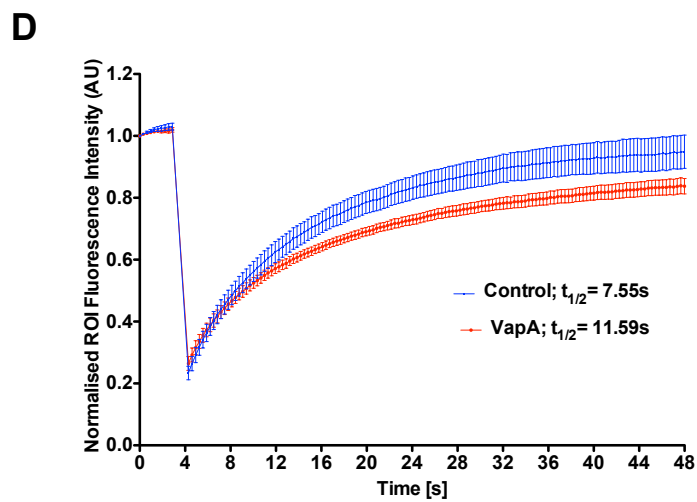
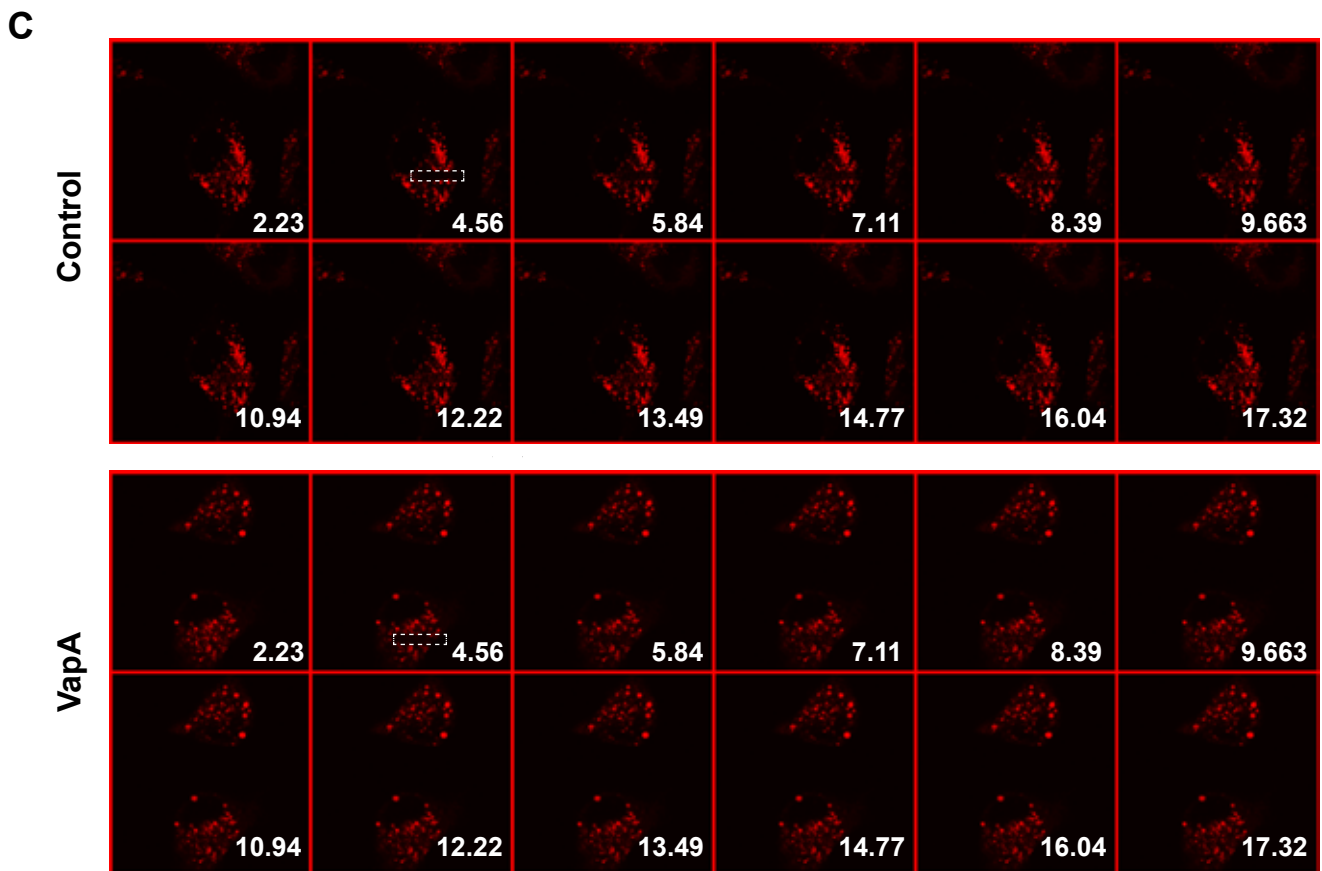
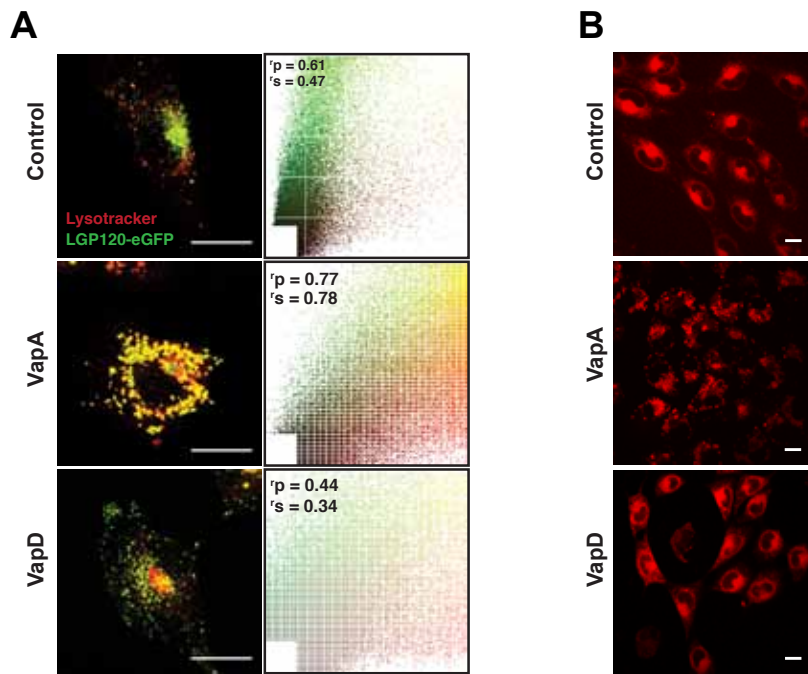


**Fig. 6**

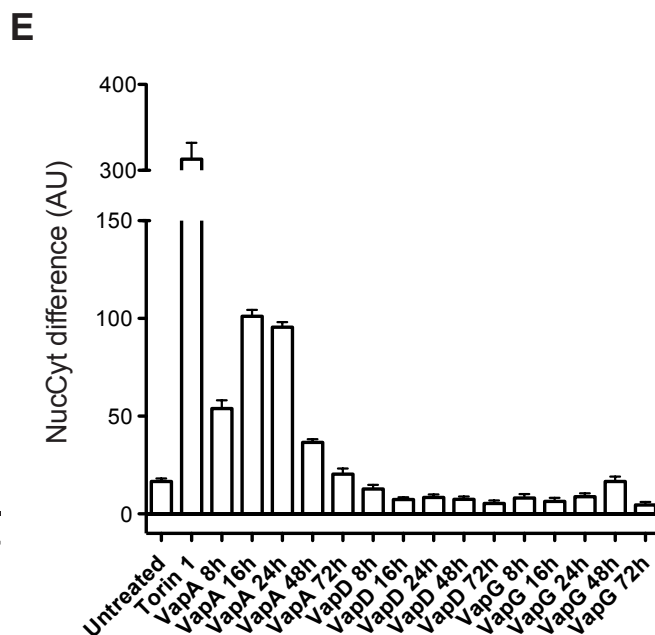
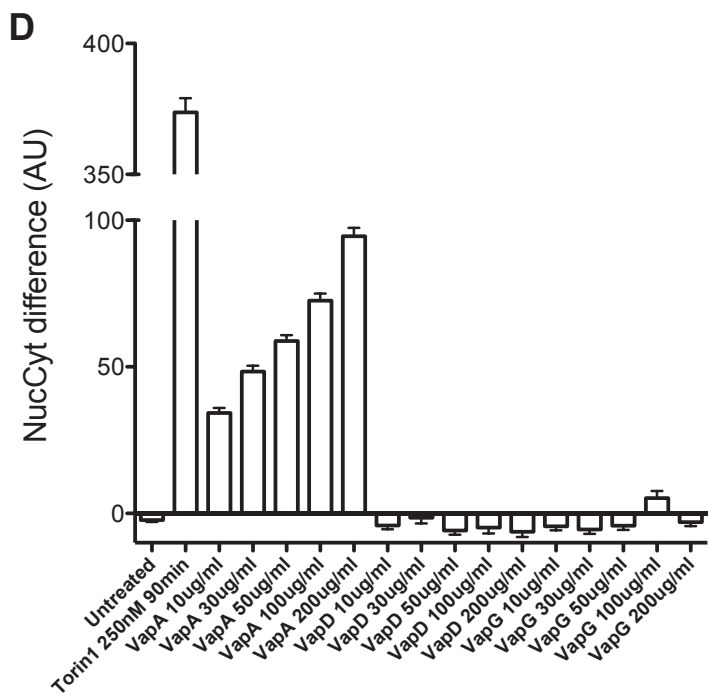
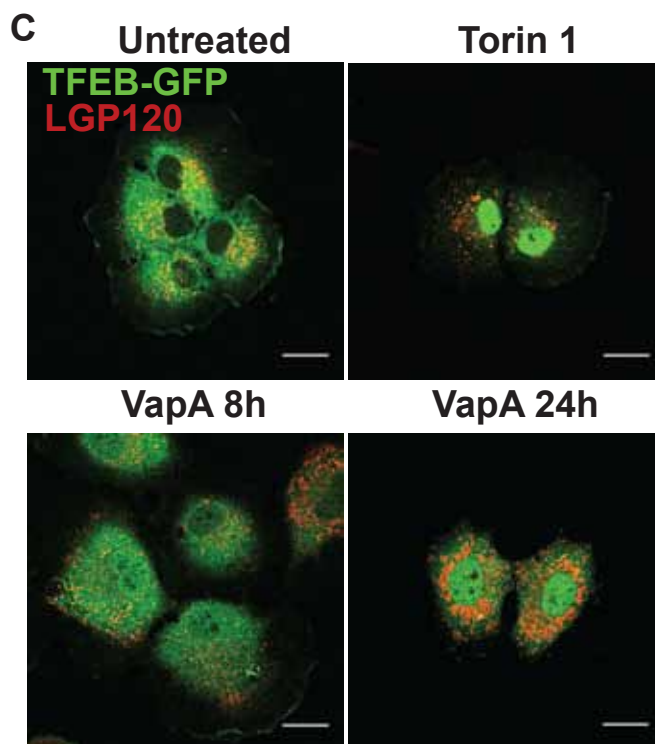
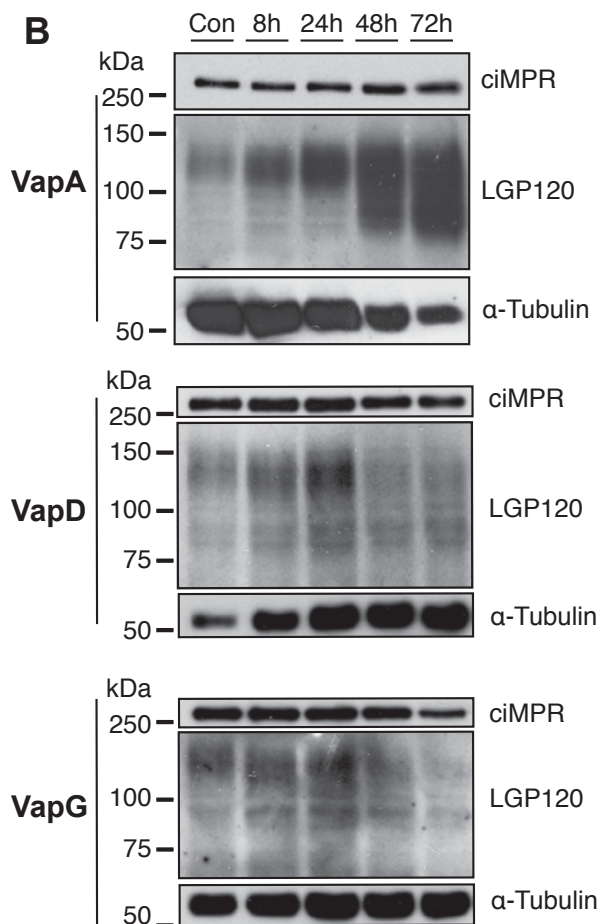
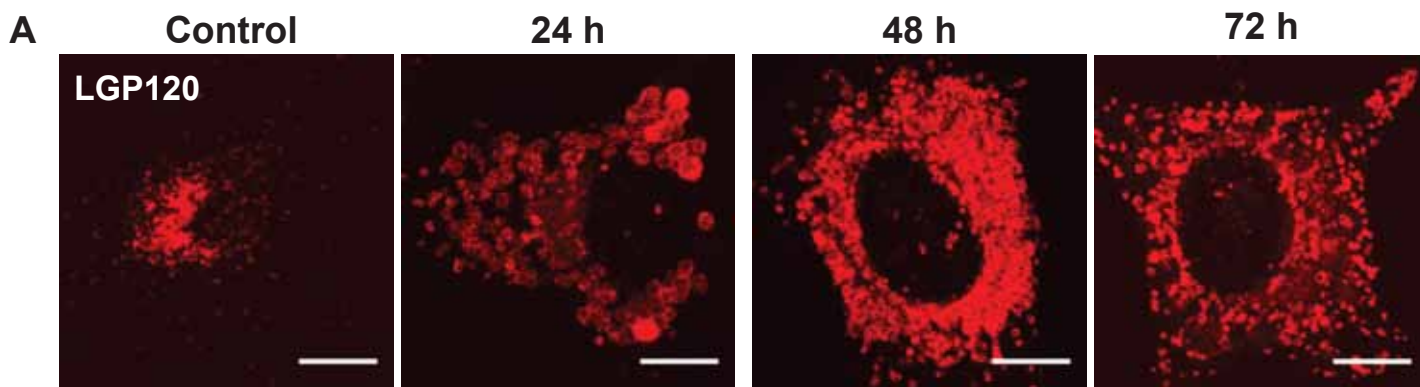


**Fig. 7**

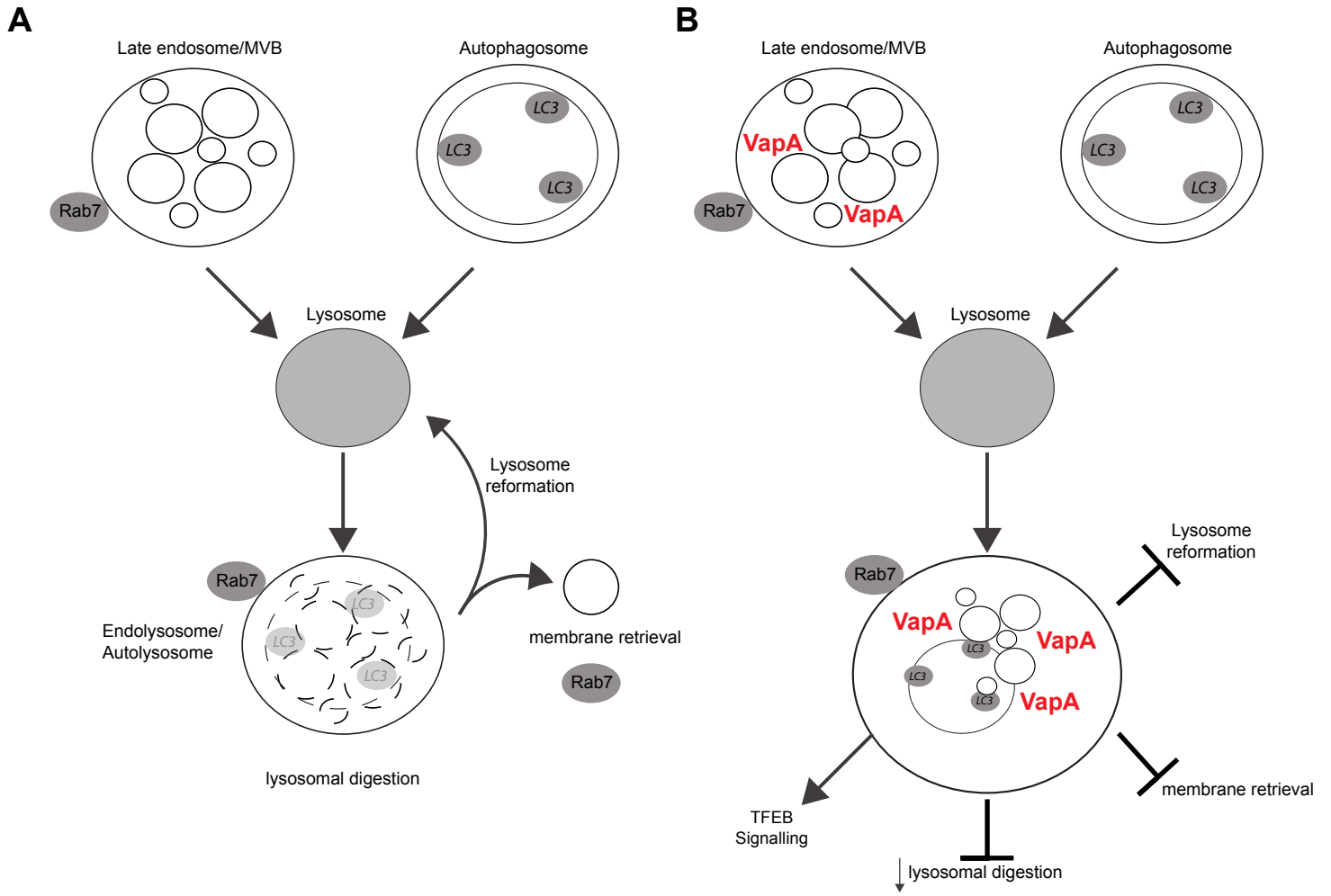


**Fig. 8**

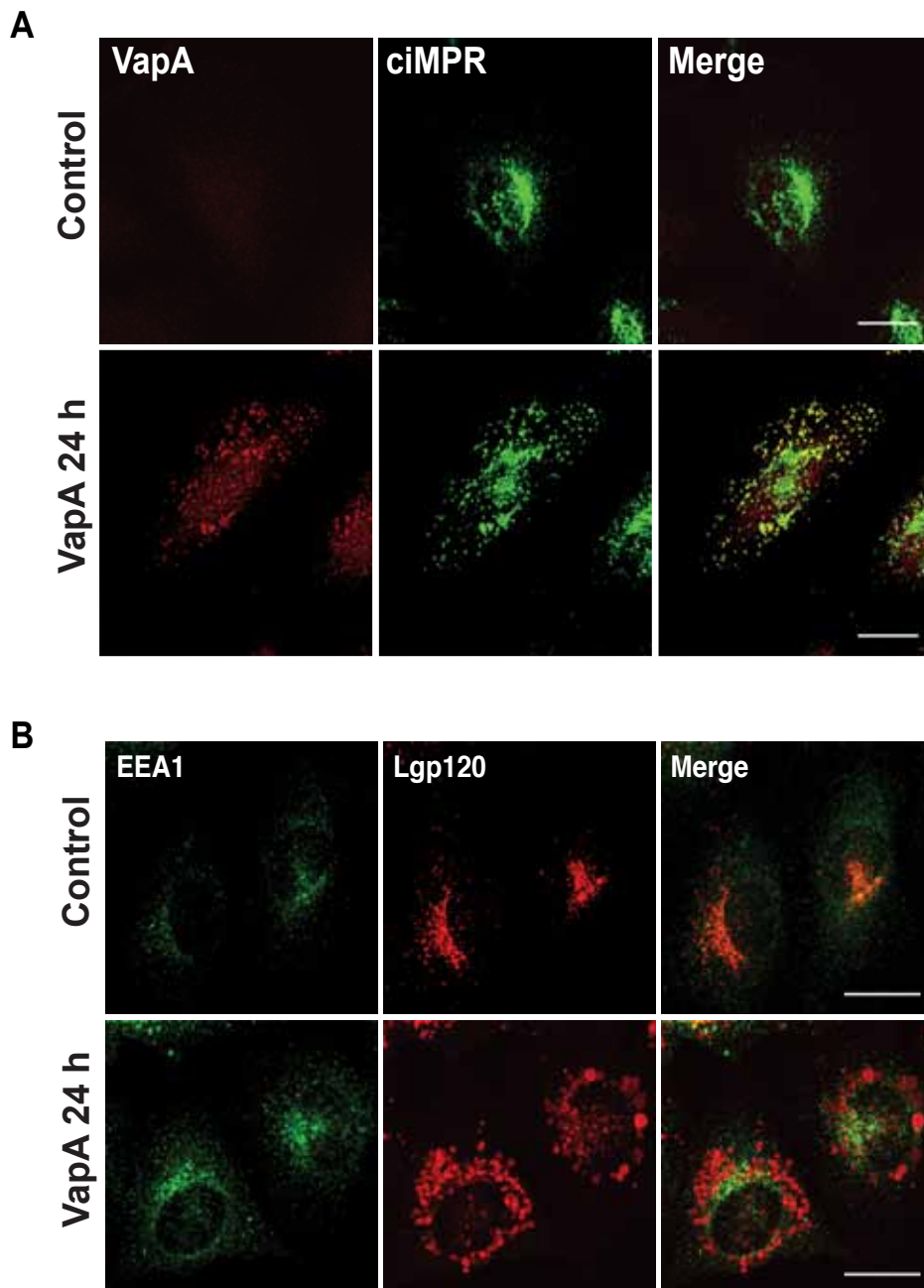


Fig. S1

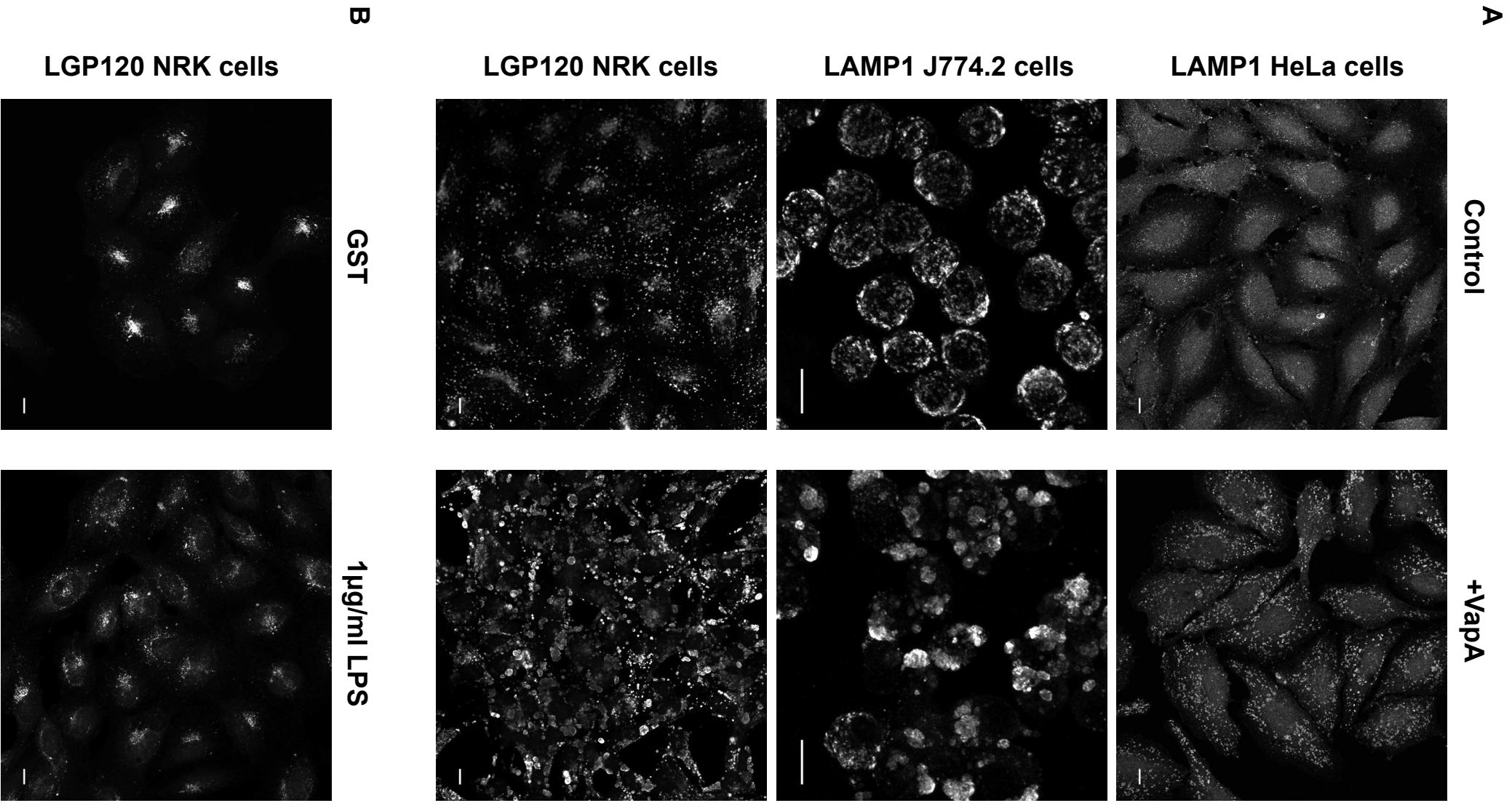


Fig.S2

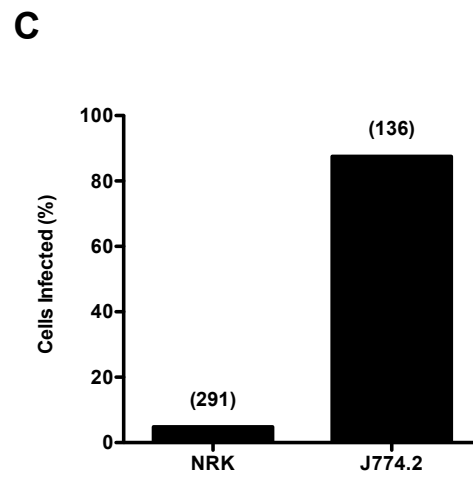
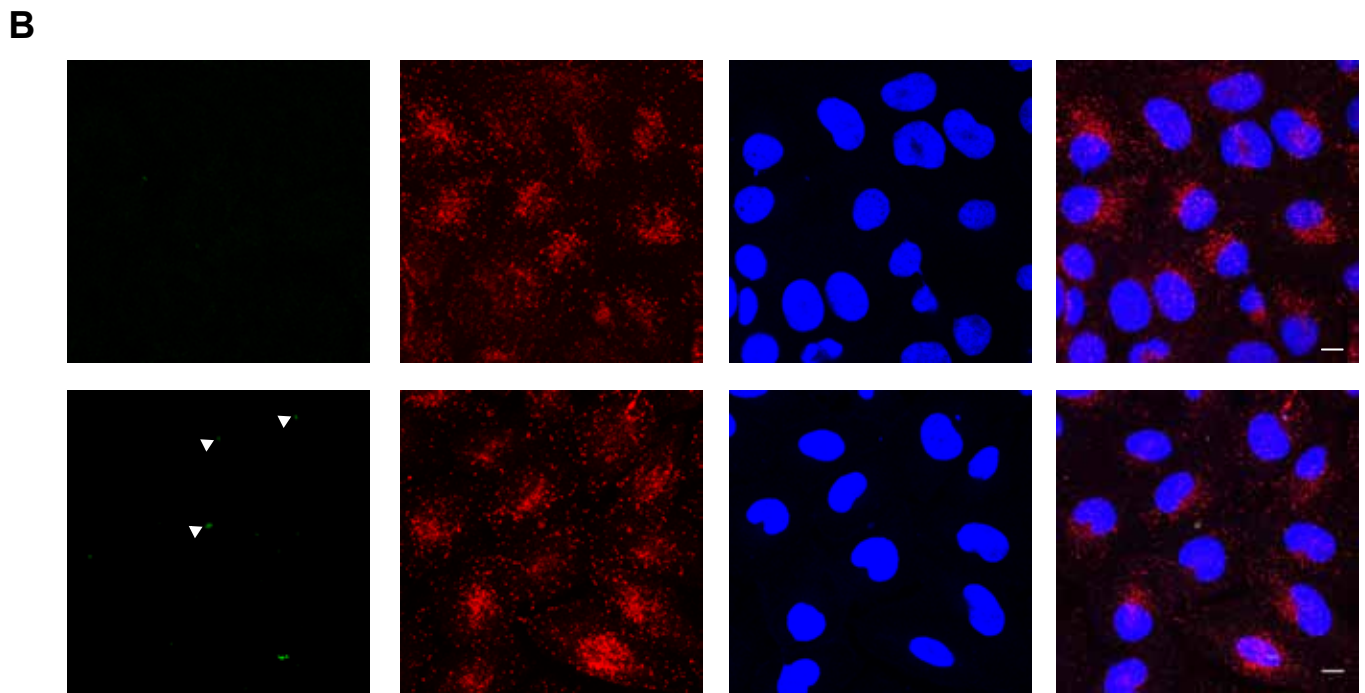
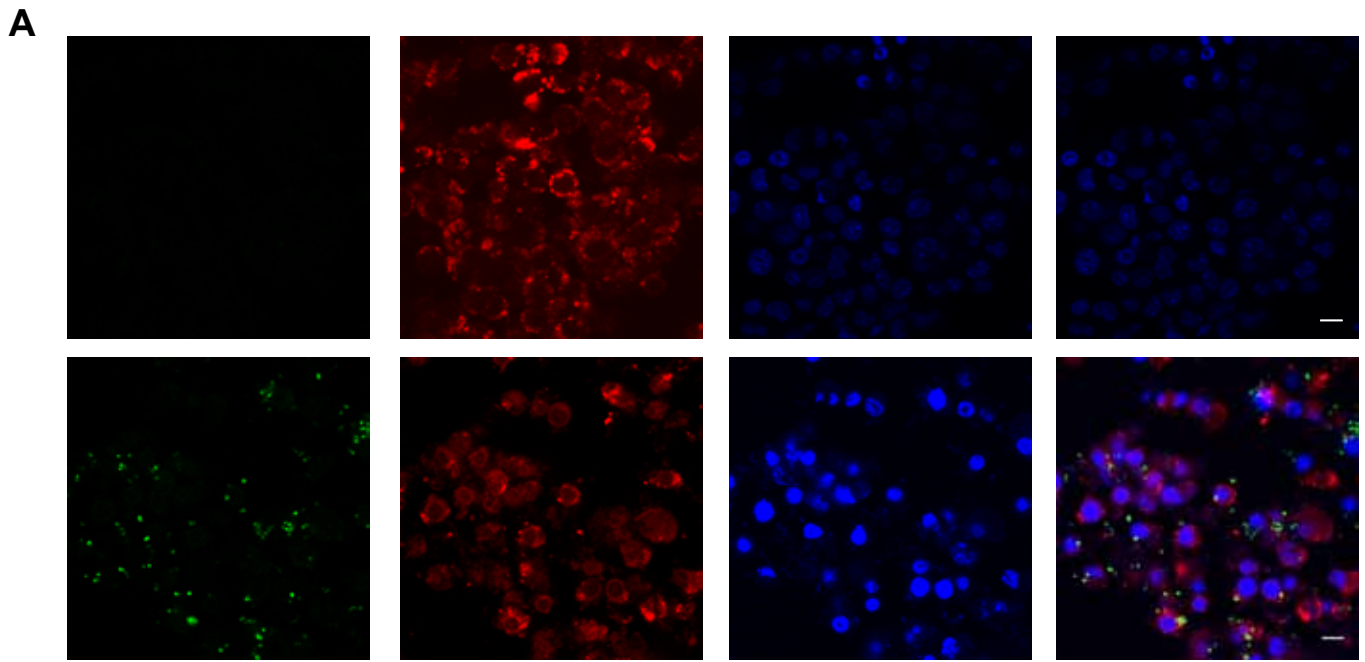
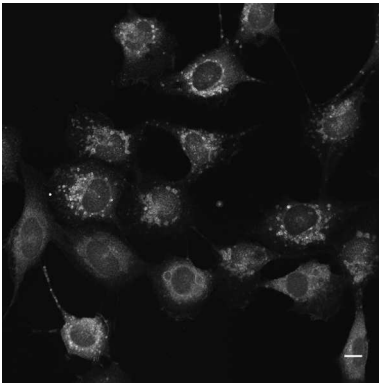


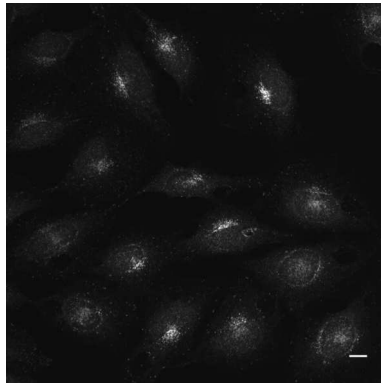
Fig. S3

**A**

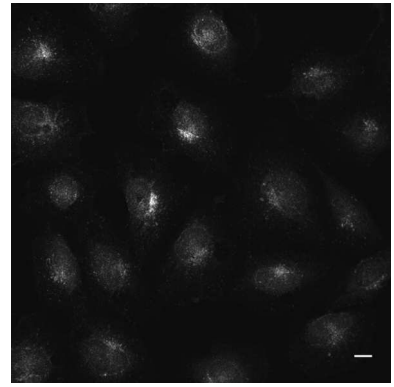
**VapA**



**VapD**

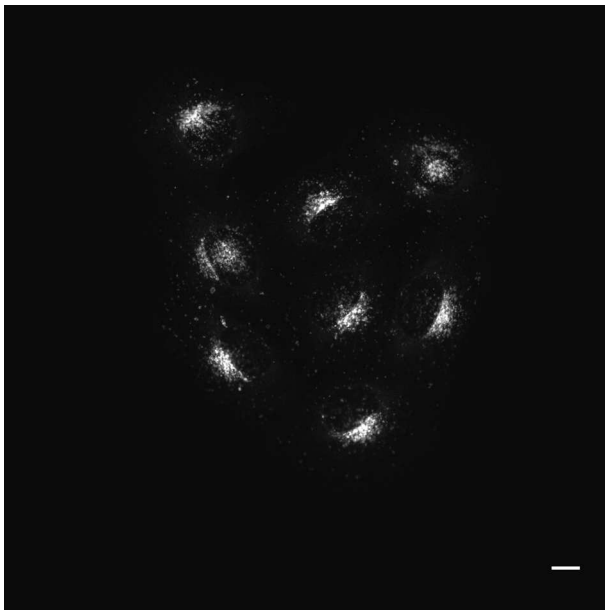


**VapG**

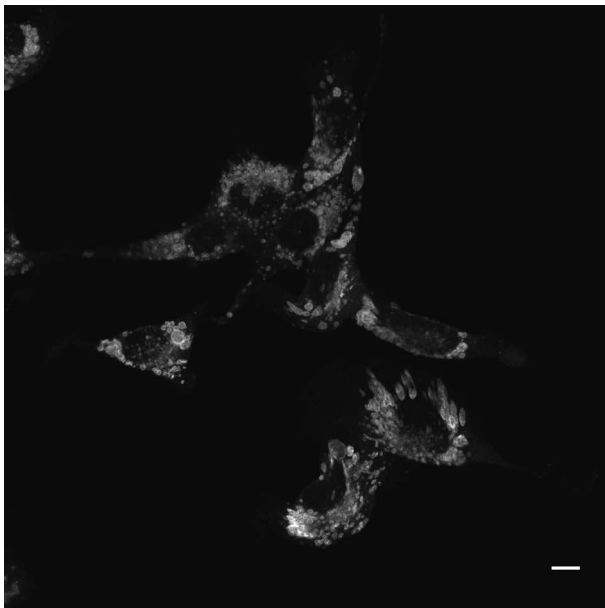
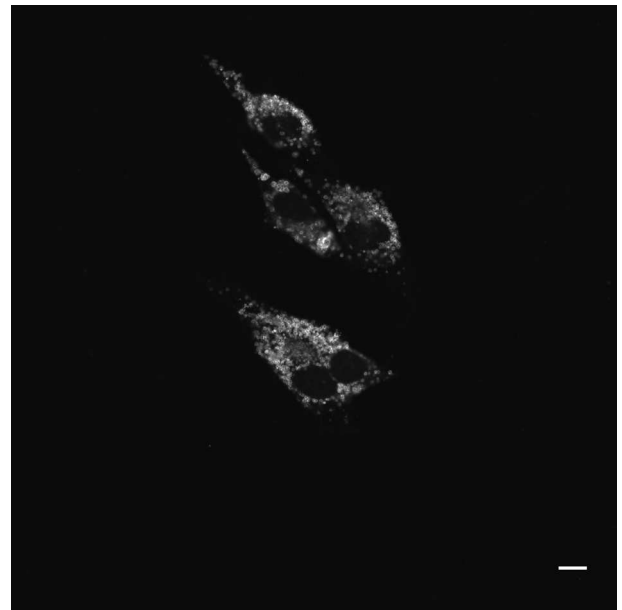


**B**

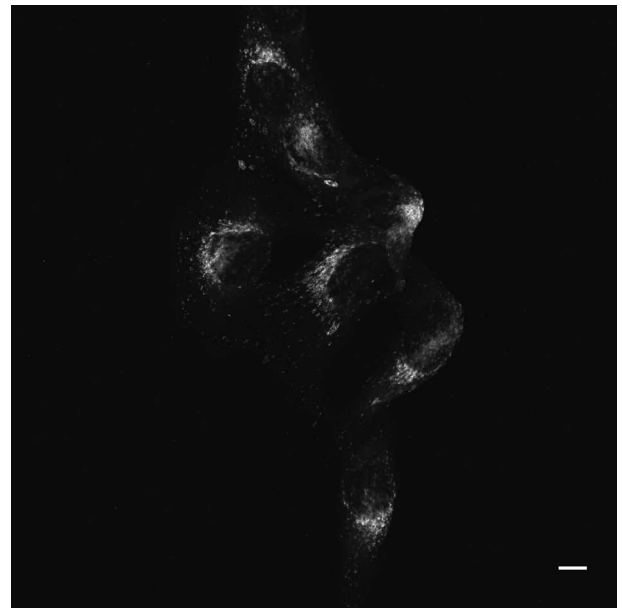
**Control**



**VapA Core**



**VapDA**



**VapAD**

**Fig. S4**

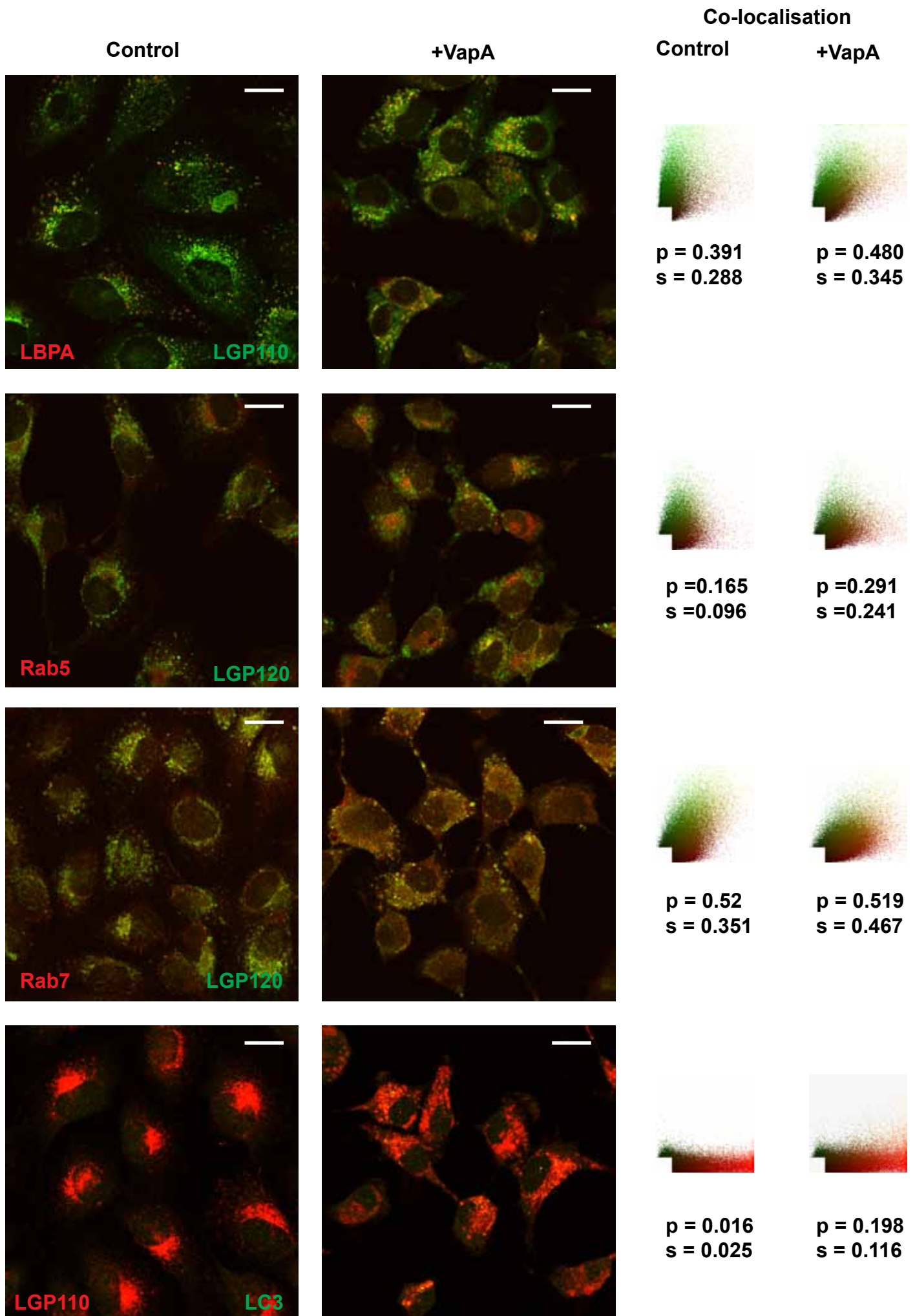


Fig. S5